Investigation of MoS_2 with Ambient Pressure X-ray Photoelectron Spectroscopy

by
Derek Dardzinski

A THESIS

submitted to

Oregon State University

Honors College

in partial fulfillment of
the requirements for the
degree of

Honors Baccalaureate of Science in Chemical Engineering
(Honors Associate)

Presented May 28, 2020
Commencement June 2020

AN ABSTRACT OF THE THESIS OF

Derek Dardzinski for the degree of Honors Baccalaureate of Science in Chemical Engineering presented on May 28, 2020. Title: Investigation of MoS_2 with Ambient Pressure X-ray Photoelectron Spectroscopy.

Abstract approved:_____

Gregory Herman

Molybdenum disulfide (MoS_2) has potential applications as a low-cost catalyst for the hydrogen evolution reaction (HER). Defects on MoS_2, such as edge sites and sulfur vacancies, are known to be the major active sites for HER. Controlling the formation of these defects allows for the enhancement in reactivity of MoS_2 and other 2D materials. In this study, we have characterized the surface reactivity of bulk MoS_2 samples using ambient pressure X-ray photoelectron spectroscopy (APXPS). Samples were exposed to 1 mbar of H_2O vapor at temperatures ranging from 300-600 K. The APXPS Mo 3d, S 2p, and O 1s core levels for the as exfoliated surface showed no significant changes under all reaction temperatures due to the inert nature of the pristine MoS_2 surface. To improve surface reactivity and activate the basal plane of MoS_2 we have utilized Ar+ sputtering to form well controlled defect densities at the surface. The APXPS Mo 3d, S 2p, and O 1s core levels for the defective MoS_x (x = 1.6, 1.4, 1.2) surface showed the formation of MoO_3 and MoOS at temperatures of 400 K and above. We have found that surface reactivity of MoS_2 is strongly dependent on temperature and defect densities.

Key Words: MoS_2, Ambient Pressure X-ray Photoelectron Spectroscopy, Surface Science

Corresponding e-mail address: dardzind@oregonstate.edu

Investigation of MoS_2 with Ambient Pressure X-ray Photoelectron Spectroscopy

by
Derek Dardzinski

A THESIS

submitted to

Oregon State University

Honors College

in partial fulfillment of
the requirements for the
degree of

Honors Baccalaureate of Science in Chemical Engineering
(Honors Associate)

Presented May 28, 2020
Commencement June 2020

Honors Baccalaureate of Science in Chemical Engineering project of Derek Dardzinski presented on May 28, 2019.

APPROVED:

_____

Gregory Herman, Mentor, representing Chemical Engineering

_____

Rafik Addou, Committee Member, representing Chemical Engineering

_____

Kelsey Stoerzinger, Committee Member, representing Chemical Engineering

_____

Toni Doolen, Dean, Oregon State University Honors College

I understand that my project will become part of the permanent collection of Oregon State University, Honors College. My signature below authorizes release of my project to any reader upon request.

_____

Derek Dardzinski, Author

Table of Contents

1. Introduction

1.1 Two Dimensional Materials

Layered, two-dimensional (2D) materials[1] consist of monolayers held together via weak Van der Waals interactions. The unique electrical properties that arise from this layered structure make 2D materials attractive candidates for many applications such as electronics, optoelectronics, and catalysis.[2–4] Graphene, a monolayer of carbon atoms, was the original 2D material that gained recognition from the scientific community.[5] The vast potential of graphene led to the increased interest in materials such as two-dimensional transition metal dichalogenides (2DTMDs), hexagonal boron nitrides, metal oxides and more.[5] Additionally, heterostructures made from layers of different materials have been developed which have unique and tunable properties.[6] The structure of each material described above can be seen in figure 1. The number of unique 2D materials is ever expanding, but the main focus of this study is on molybdenum disulfide (MoS_2), a 2DTMD material. The layered structure of MoS2 shown above is made from a layer of molybdenum atoms sandwiched between two layers of sulfur atoms. The next section will describe how this structure can be engineered for optimal electocatalytic performance.

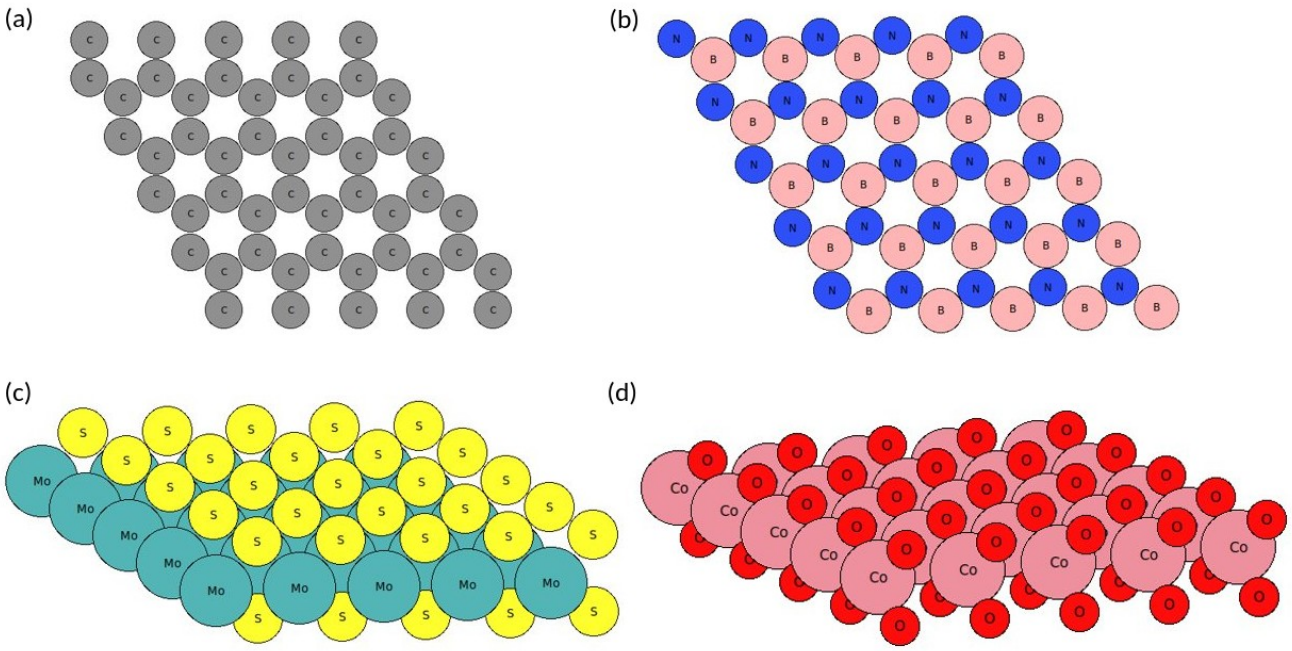

Figure 1.1.1: Visualizations of four different 2D crystal structures. **(a)** graphene, honeycomb structure **(b)** hexagonal boron nitride, honeycomb structure **(c)** MoS_2, hexagonal structure **(d)** CoO_2, orthorhombic structure

1.2 Tailoring Defects for 2D Electrocatalysis Applications

Electrocatalysis can be defined as "the heterogeneous catalysis of electrochemical reactions, which occur at the electrode-electrolyte interface and where the electrode plays both the role of electron donor/acceptor and of the catalyst".[7] From this definition, it is clear that an ideal electrocatalyst would have a large active surface area, high chemical activity, and high electrical conductivity to easily accept and donate electrons to adsorbates. Platinum has been the standard for electocatalysis for many years, however its expensive price, and limited abundance, has driven the demand for cheaper and more available materials. One of many alternatives are 2DTMDs as described in section 1.1. Their relatively inexpensive price, and chemically active edges[8] make them attractive for electrocatalysis applications. However, due to the layered structure of 2DTMDs, the basal plane of the material is chemically inert due to the lack of dangling bonds at the surface.[8] This dramatically reduces

the active surface area, therefore requiring defects to be engineered on the surface to create more chemically active sites.

The basal plane of 2DTMDs such as MoS_2 is commonly activated through the creation of anion vacancies at the surface.[2] This type of defect is thermodynamically favorable due to its low formation energy and can be created easily through ion sputtering and annealing.[9] Anion vacancies in MoS_2 move the valence and conduction bands closer to the Fermi level,[9] decreasing the energy required for electron transfer, an important mechanistic step in the hydrogen evolution reaction (HER).[10] Additionally, the local conductivity of the anion vacancy site is increased, improving the charge mobility which benefits the HER activity.

Heteroatom dopants have also been shown to increase the electrochemical activity of 2DTMDs. Specifically for MoS_2, nitrogen and phosphorous dopants are promising candidates for increasing HER activity because of the boost in conductivity created by the additional electrons from the dopant atoms.[11] In another mechanism similar to that of anion vacancies, adatoms and dopants of certain metals such as platinum on MoS_2 can reduce the band gap and create new gap states which lower the free energy of hydrogen absorption for HER.[4]

Of the two defect categories mentioned above, this study will focus on the influence of anion vacancies on the chemical activity of MoS_2. The effects of dopants will be saved for another study.

2. Experimental Methods

2.1 Materials

Bulk MoS_2 was purchased from HQ Graphene. Water vapor was generated from deionized (DI) water (18.2 MΩ cm^{-1}). 3M scotch tape was used for mechanical exfoliation after which the sample was immediately loaded to a UHV loadlock with a base pressure of $3x10^{-8}$ mbar. Each sample was approximately 3 mm x 5 mm.

Figure 2.1.1: Image of MoS_2 sample purchased from HQ Graphene

2.2 Creation of Defects

The natural MoS_2 surface was mechanically exfoliated with scotch tape before entering the load lock chamber. To induce defects on the surface, 99.9% Ar gas was used to sputter the sample for 5, 15, and 18 minutes with 1 kV of argon ions (Ar^+) with a spot size of 10 mm x 10 mm with raster mode and an emission current of 10 mA, resulting in varying densities of sulfur vacancies/voids at the top most layers of MoS_2.

2.3 X-ray Photoelectron Spectroscopy

X-ray photoelectron spectroscopy (XPS) was performed using the SPECS ambient pressure XPS system (APXPS) with a monochromatic Al Kα ($h\nu$ = 1486.6 eV) X-ray source, hemispherical analyzer, ultra high vacuum chamber with a base pressure of ~ $2x10^{-10}$ mbar, and a differentially pumped ambient pressure analyzer. Spectra were obtained with a 35.0 eV analyzer pass energy, 0.1 eV energy step size, and 4 scans until a reasonable signal-to-noise ratio was obtained. Fitting of the APXPS spectra was performed in CasaXPS using Gaussian-Lorenzian peak shapes with a linear background for the C1s and O1s core levels, and a Shirley background for the Mo3d and S2p core levels. For the Mo3d core level, the MoS_2 peak can be fit with a GL(60) peak shape and a full width half-max (FWHM) of 0.7 eV for the $3d_{5/2}$ peak and 0.8 eV for the $3d_{3/2}$ peak. Metallic molybdenum has an asymmetric peak shape of LA(1.1,2.3,2). Spin orbit splitting for the Mo3d core level is 3.13 eV between $Mo3d_{5/2}$ and $Mo3d_{3/2}$ peaks, and spin orbit splitting for the S2p core level 1.18 eV between the $S2p_{3/2}$ and $S2p_{1/2}$ peaks.[12] Sensitivity factors (S) were calculated assuming a homogeneous sample, and that the analyzer and X-ray flux are equal allowing the equation to simplify to what is seen in *Equation 1*. The effective attenuation length (Λ_i) was calculated using *Equation 2*,[13] and the differential photoionization cross section ($d\sigma_i/d\Omega_i$) was calculated using *Equation 3*.[14] Cross section (σ_i) and asymmetry parameter values (β_i) were obtained from calculated tables.[15,16] The kinetic energy (E) is taken from the most intense peak present in the core level spectrum. (Z) is the average atomic number of MoS_2, the lattice parameter (a) is calculated using *Equation 4*[13] where ρ is the density of the material. The angle between the X-ray source and the analyzer (α) is 60 degrees.

$$S = \Lambda_i \left(\frac{d\sigma_i}{d\Omega_i} \right) \quad \text{(Equation 1)}$$

$$\Lambda_i = 0.316 a^{3/2} \left[\frac{E}{Z^{0.45} \left[\ln\left(\frac{E}{27}\right) + 3 \right]} + 4 \right] \quad \text{(Equation 2)}$$

$$\frac{d\sigma_i}{d\Omega_i} = \frac{\sigma_i}{4\pi} \left[1 + \frac{\beta}{2} \left(\frac{3}{2} \sin^2(\alpha) - 1 \right) \right] \quad \text{(Equation 3)}$$

$$a = 10^8 \left(\frac{\mu}{\rho N_A} \right)^{1/3} \quad \text{(Equation 4)}$$

2.4 Atomic Force Microscopy

Atomic force microscopy (AFM) was performed using a Bruker Veeco diInnova AFM using standard tapping mode with a 300 kHz, 40 N/m, 125 μm long, 30 μm width, and < 10 nm radius cantilever (Budget Sensors Tap300Al-G). Scans were collected at a scan rate of 1 Hz containing 256x256 taps. AFM images were analyzed using the software WSxM to determine the root mean squared roughness of the surface.

3. Results and Discussion

3.1 Ar^+ Ion Sputtering

To show that the presence of defects on the surface of MoS_2 can increase the chemical activity of the basal plane, argon ion sputtering was employed to preferentially remove sulfur atoms from the top layer of the surface. This behavior can be seen in the data from the decrease in the S:Mo stouchiometric ratio. As discussed in *Section 1.2*, sulfur vacancies are known to increase the HER activity of MoS_2. For this study, three different defective surfaces were created with S:Mo ratios of 1.6:1, 1.4:1, and 1.2:1. This section will discuss the results of argon ion sputtering for each defect density.

The least defective 1.6:1 surface was created using 15 total minutes of argon ion sputtering at an energy of 1 kV after the surface was mechanically exfoliated. In *Figure 3.1.1* the evolution of the Mo3d XPS core-level spectrum is shown with respect to sputtering time. The clear lower binding energy shoulders, and general broadening in the Mo3d core-level spectra was caused by the presence of sulfur defects and the formation of metallic molybdenum which create available bonding sites for adsorbates like water to react.

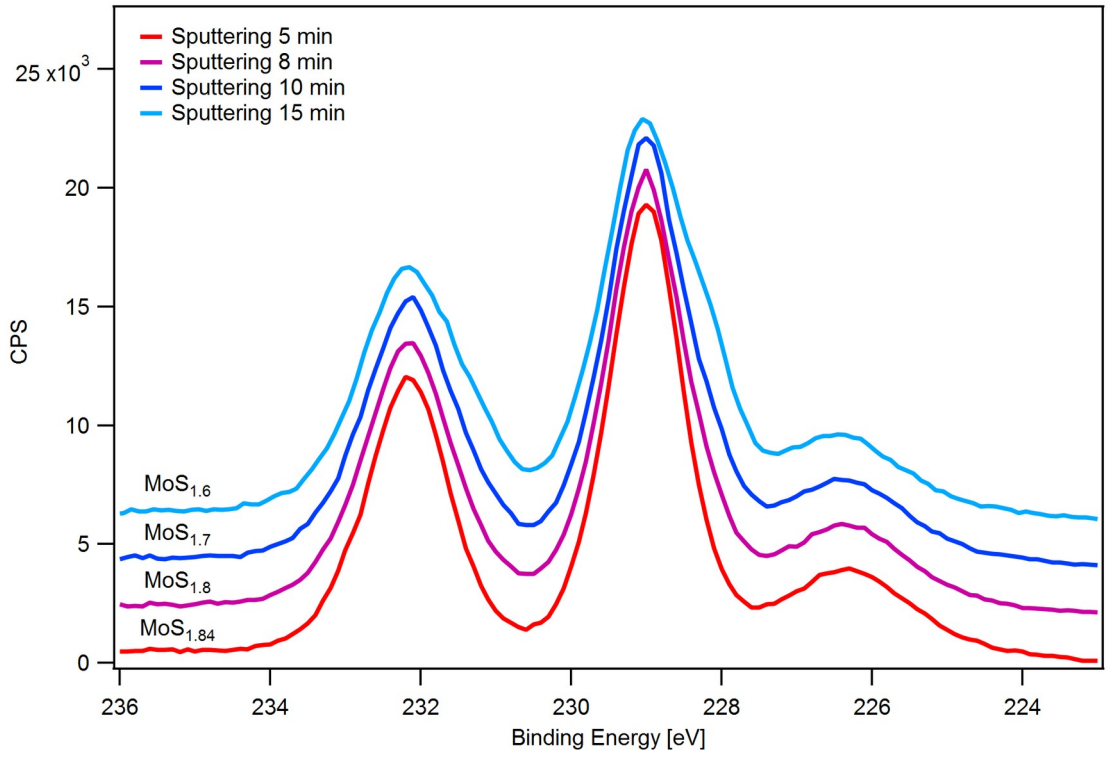

Figure 3.1.1: Mo3d core level XPS spectra of an MoS_2 surface while being sputtered with 1 kV of Ar^+ ions for 5, 8, 10, and 15 minutes. There was a clear broadening of the peaks as sputtering time increased. The lower binding energy shoulder that developed on the $Mo3d_{5/2}$ and $Mo3d_{3/2}$ peaks came from the presence of sub-stoichiometric MoS_2 and metallic molybdenum, Mo(0).

In *Figure 3.1.2a* the surface composition percentages of MoO_3, MoS_x, MoS_2, and Mo(0) are plotted with respect to sputtering time. A clear increase in the presence of sub-stoichiometric MoS_x was seen as well as an increase in Mo(0) which both attribute to the lower binding energy shoulders discussed above. The decrease in MoS_2 shows that the surface layers of MoS_2 are transitioning to sub-stoichiometric MoS_x. There was also a slight decrease in the MoO_3 during the sputtering process. In *Figure 3.2.1b,* calculated ratios of all detected chemical species are shown with respect to sputtering time. The S:Mo ratio for the sulfur deficient MoS_x decreased to 1.6:1 after 15 minutes of sputtering, and the O:Mo ratio for MoO_3 decreased to 1.7:1. The S:Mo ratio of MoS_2 remained at a constant 2:1 because the signal was originating from the bulk of the sample the areas unaffected by the argon sputtering.

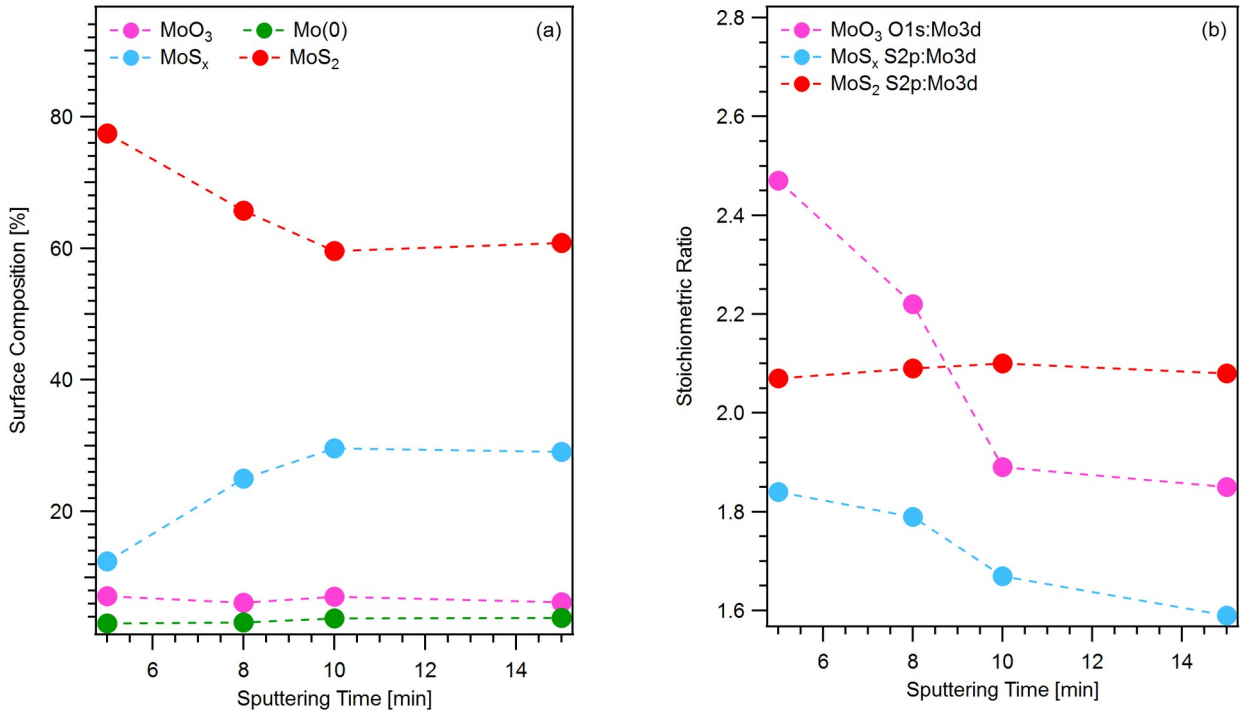

Figure 3.1.2: (a) Calculated surface composition percentages for MoS_2 (red), MoS_x (light blue), MoO_3 (pink), and Mo(0) (green) while being sputtered with 1 kV of Ar^+ ions. There was a large increase in the sub-stoichiometric MoS_x present on the surface showing that sputtering removed sulfur atoms from the surface, consequently there was an increase in Mo(0) on the surface showing the formation of metallic molybdenum. MoO_3 also decreased since it was being removed by the Ar^+ sputtering. **(b)** Calculated stoichiometric ratios of MoO_3 (O:Mo), MoS_2 (S:Mo), and MoS_x (S:Mo). Large decreases in stoichiometry were seen for both MoO_3 and MoS_x. The final MoS_x (S:Mo) stoichiometry was 1.6:1. MoS_2 remained constant because its signal comes from the bulk of the material.

The next surface created was the 1.4:1 surface, which should show more prominent lower binding energy shoulders as more defect sites and metallic molybdenum was created. *Figure 3.1.3* shows the Mo3d core-level XPS spectra with respect to sputtering time. The development of a strong lowering binding energy shoulder was seen after only 5 minutes of sputtering. This surface was expected to be more reactive when exposed to 1 mbar of water vapor because more defect sites were present, which in turn means more available active sites.

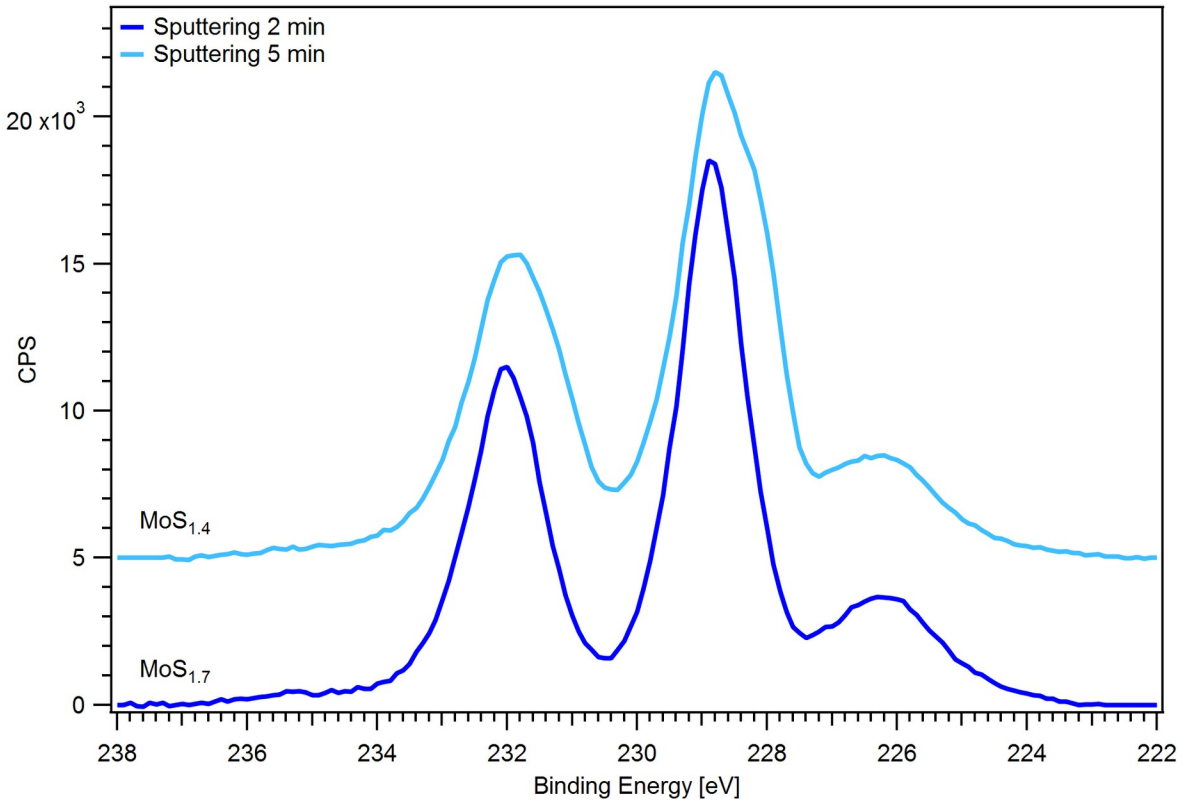

Figure 3.1.3: Mo3d core level XPS spectra of an MoS_2 surface while being sputtered with 1 kV of Ar^+ ions for 2 and 5 minutes. There was a clear broadening of the peaks as sputtering time increased. The lower binding energy shoulder that developed on the $Mo3d_{5/2}$ and $Mo3d_{3/2}$ peaks came from the presence of sub-stoichiometric MoS_2 and metallic molybdenum, Mo(0).

In *Figure 3.1.4a* the surface composition percentages of MoS_x, MoS_2, and Mo(0) were plotted with respect to sputtering time. Similar to the 1.6:1 surface, there was an increase in the MoS_x surface percentage, as well as the metallic molybdenum. There was no preexisting MoO_3 on the surface, which might explain why there was less sputtering time required to create a more defective surface. In *Figure 3.1.4b,* calculated ratios of all detected chemical species are shown with respect to sputtering time. The S:Mo ratio for the sulfur deficient MoS_x decreased to 1.4:1 after 5 minutes of sputtering. The S:Mo ratio of MoS_2 again remained at a constant 2:1.

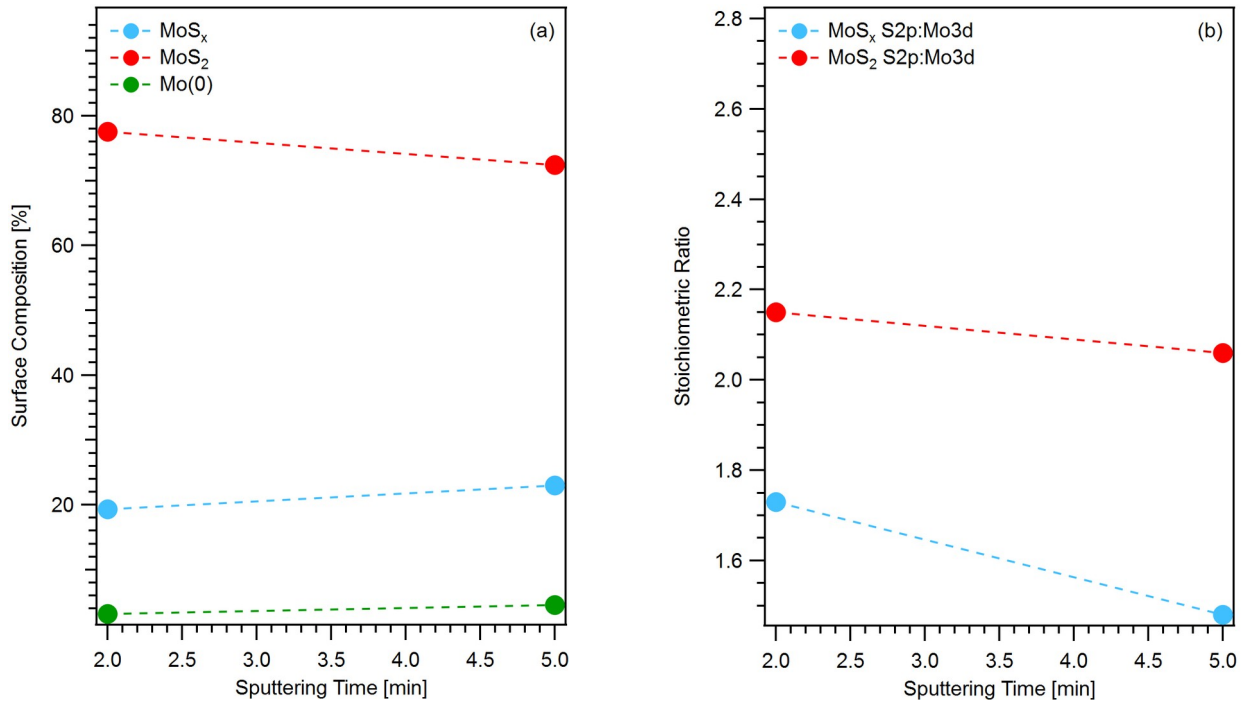

Figure 3.1.4: (a) Calculated surface composition percentages for MoS_2 (red), MoS_x (light blue), MoO_3 (pink), and Mo(0) (green) while being sputtered with 1 kV of Ar^+ ions. There was an increase in the sub-stoichiometric MoS_x present on the surface as well as an increase in Mo(0) showing the formation of metallic molybdenum. **(b)** Calculated stoichiometric ratios of MoS_2 (S:Mo), and MoS_x (S:Mo). A large decrease in stoichiometry was seen for MoS_x. The final MoS_x (S:Mo) stoichiometry was 1.4:1.

The last surface created was the 1.2:1 surface, which showed the most prominent lower binding energy shoulders and had the most defect sites and metallic molybdenum. *Figure 3.1.5* shows the Mo3d core-level XPS spectra with respect to sputtering time. Strong lowering binding energy shoulder were again seen after a total of 18 minutes of sputtering. This surface is predicted to be the most reactive because of the high amounts of defects.

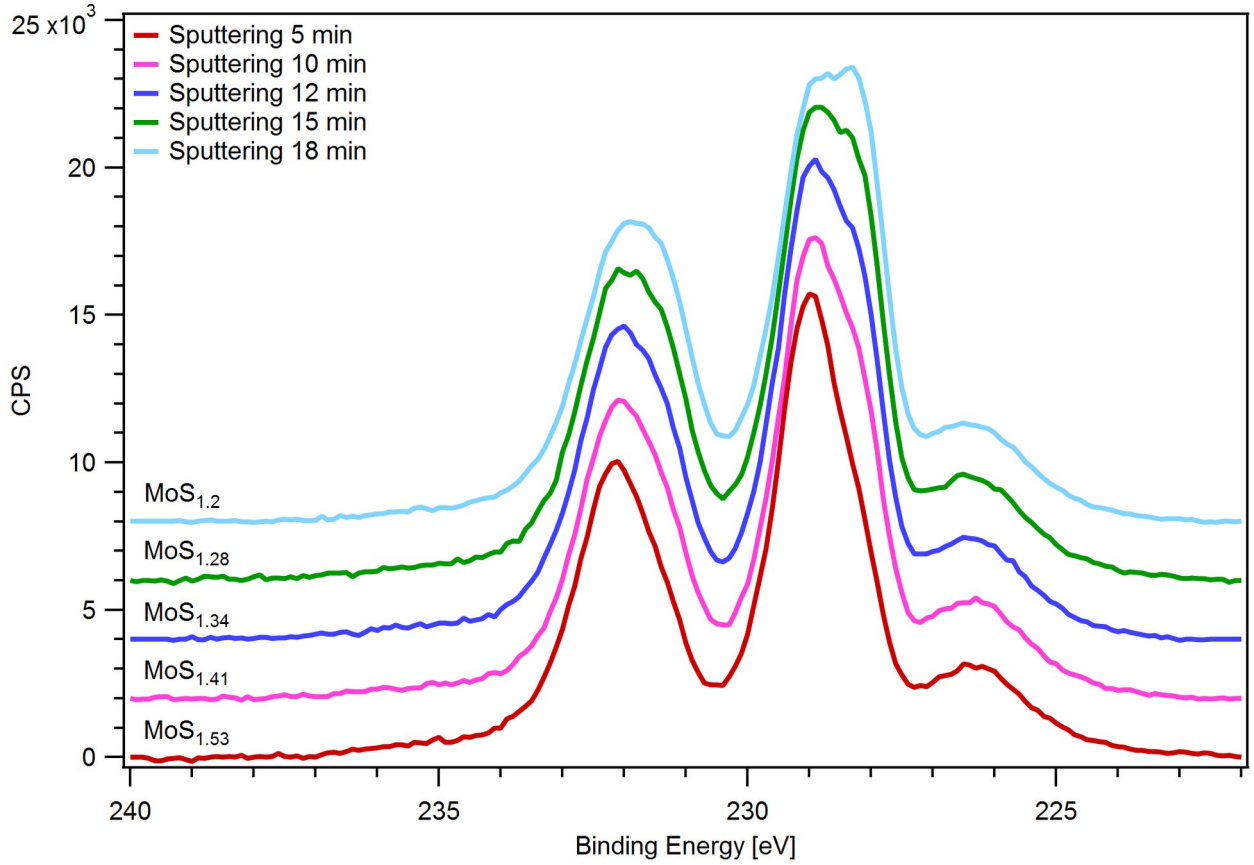

Figure 3.1.5: Mo3d core level XPS spectra of an MoS_2 surface while being sputtered with 1 kV of Ar^+ ions for 5, 10, 12, 15 and 18 minutes. There was a clear broadening of the peaks as sputtering time increased. The lower binding energy shoulder that developed on the $Mo3d_{5/2}$ and $Mo3d_{3/2}$ peaks came from the presence of sub-stoichiometric MoS_2 and metallic molybdenum, Mo(0).

In *Figure 3.1.6a* the surface composition percentages of MoO_3, MoS_x, MoS_2, and Mo(0) are plotted with respect to sputtering time. The behavior was similar to the previously discussed surfaces. In *Figure 3.2.1b*, calculated ratios of all detected chemical species are shown with respect to sputtering time. The S:Mo ratio for the sulfur deficient MoS_x decreased to 1.2:1 after 18 minutes of sputtering. The S:Mo ratio of MoS_2 again remained at a constant 2:1, and the O:Mo ratio decreased to 1.7:1.

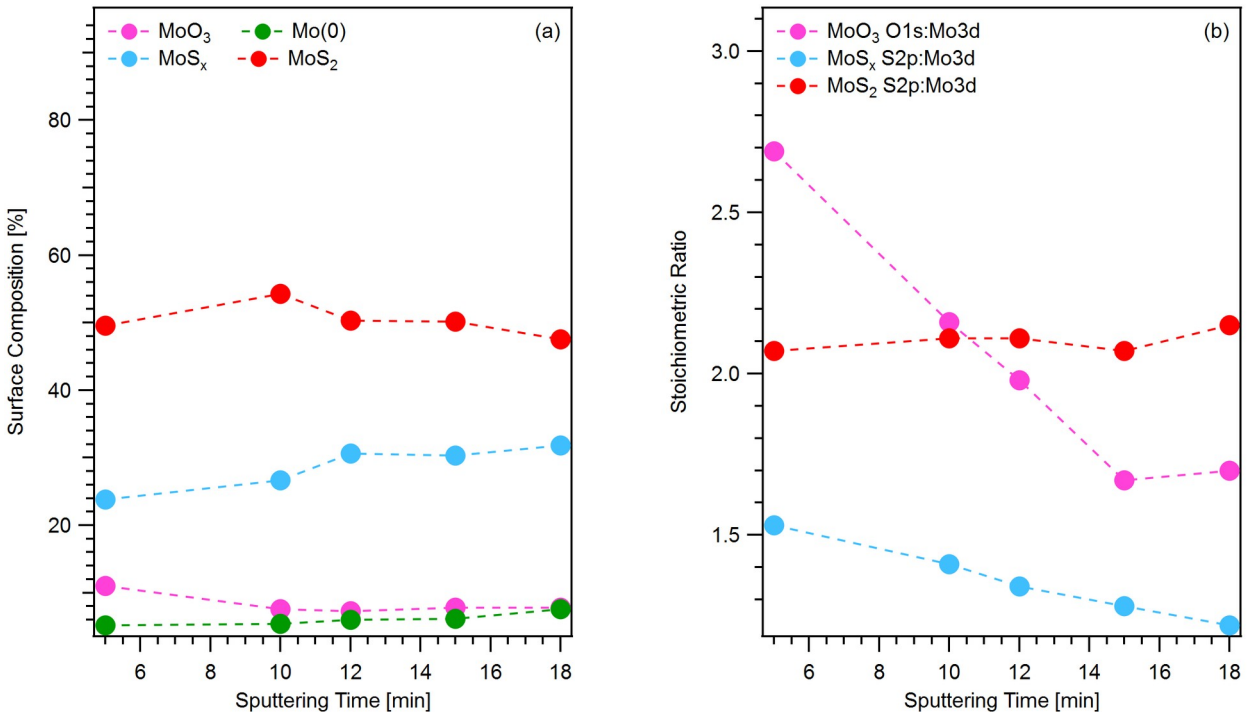

Figure 3.1.6: (a) Calculated surface composition percentages for MoS_2 (red), MoS_x (light blue), MoO_3 (pink), and Mo(0) (green) while being sputtered with 1 kV of Ar^+ ions. The MoS_x increased as sulfur was removed, while Mo(0) increased from the creation of metallic molybdenum. MoO_3 also decreased since it was being removed by the Ar^+ sputtering. **(b)** Calculated stoichiometric ratios of MoO_3 (O:Mo), MoS_2 (S:Mo), and MoS_x (S:Mo). Large decreases in stoichiometry was seen for both MoO_3 and MoS_x. The final MoS_x (S:Mo) stoichiometry was 1.2:1. MoS_2 remained constant because its signal comes from the bulk of the material.

The effect of sputtering on the RMS surface roughness of the MoS_2 surface was analyzed with AFM. A clear difference can be seen between the as exfoliated surface, and the most defective $MoS_{1.2}$ surface as the RMS roughness increased from 0.0627 nm to 0.921 nm.

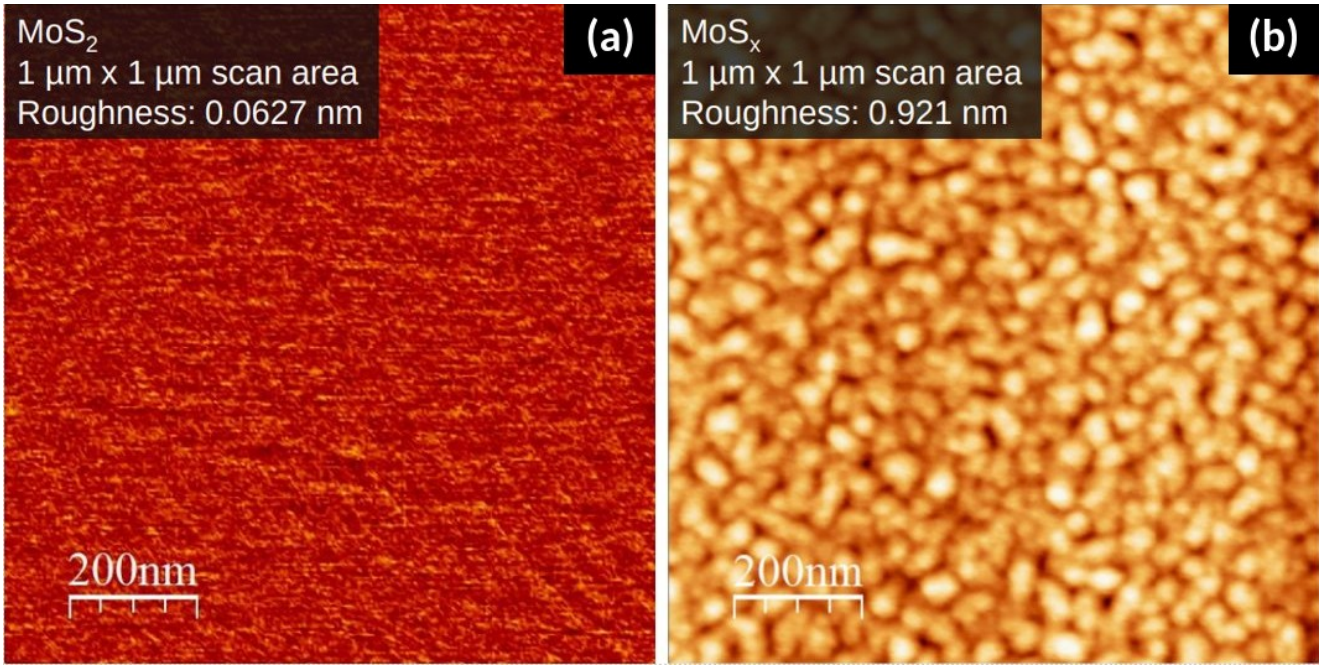

Figure 3.1.7: 1x1 micron AFM images of an MoS_2 surface before **(a)** and after sputtering and 1 mbar of water exposure **(b)**. RMS roughness is reported in the top left corner of each image.

3.2 MoS_2 Surface

To test whether the natural MoS_2 surface would oxidize in the presence of water vapor, as-exfoliated MoS_2 was exposed to 1 mbar of H_2O vapor at temperatures of 300, 400, 500, and 600 K. During this exposure the Mo3d, O1s, and S2p core level AP-XPS spectra were collected and are shown in *Figure 3.2.1*. Though there is a small presence of MoO_3 on the surface seen in the O1s ($Mo3d_{5/2}$) spectra at 530.32 eV (231.96 eV)[17] , no further growth of the MoO_3 peak was seen throughout the length of the experiment supporting what was discussed in *Section 1.2* that the natural MoS_2 surface has minimal chemical activity, especially in the presence of water. The presence of structural defects on as-exfoliated surface is responsible of this minimal reactivity of MoS2 with air and background molecules present in the UHV chamber.[18] The MoS_2 sample provided by HQ Graphene had both n-type and p-type MoS_2 present on the surface. The $Mo3d_{5/2}$ ($S2p_{3/2}$) peak for the n-type MoS_2 was at a higher binding energy of 229.26 eV (162.11 eV)[19] and the p-type $Mo3d_{5/2}$ ($S2p_{3/2}$) was located at a lower binding energy of 228.56 eV (161.41 eV). The 0.7 eV difference between the the n-type and p-type peaks is consistent with the previous results reported by Addou *et al*.[20] This n-type and p-type character remained consistent throughout all experiments. The calculated surface composition percentages of MoS_2 and MoO_3 can be seen in *Figure 3.2.2* where the percentages of MoO_3 on the surface remains mostly constant, further supporting the above conclusion that the natural MoS_2 surface is essentially chemically inert.

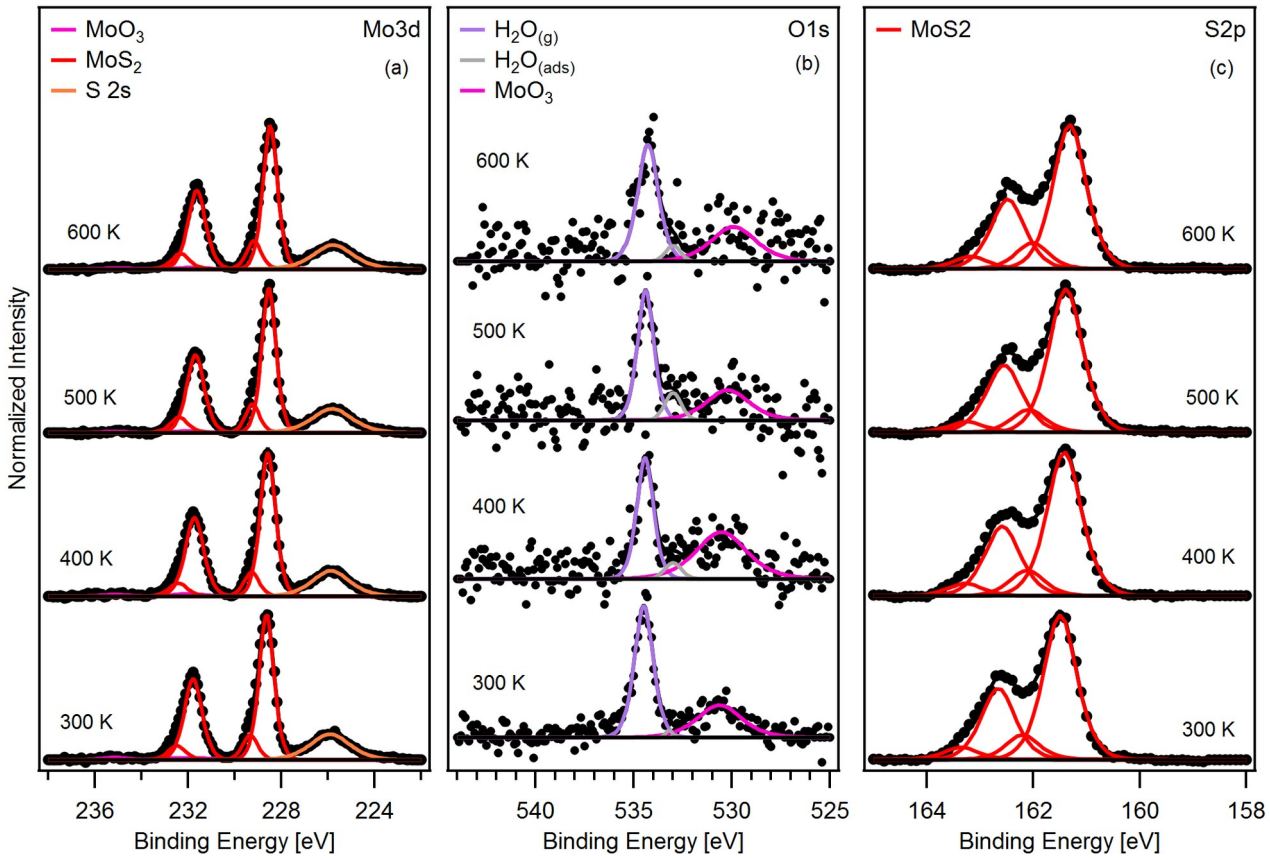

Figure 3.2.1: AP-XPS spectra of an exfoliated MoS_2 surface under 1mbar of water vapor at temperatures of 300, 400, 500, and 600 K. **(a)** shows the Mo3d core level, **(b)** shows the O1s core level, **(c)** shows the S2p core level. Red peaks represent the MoS_2 species on the surface, the higher binding energy peaks are n-type MoS_2 and lower binding energy is p-type MoS_2. Blue peaks represent MoO_3 on the surface and present themselves at high binding energies in the Mo3d core level spectra. Purple peaks represent the presence of water. The dominant peak is gas phase H_2O and the secondary peak at lower binding energies is adsorbed H_2O on the surface. As expected, the MoS2 surface does not oxidize further while exposed to the 1 mbar of H_2O.

Table 3.2.1: Binding energies of the $Mo3d_{5/2}$, $S2p_{3/2}$, and O1s peaks in *Figure 3.2.1*. The average binding energy was calculated from the fitted spectra at 300, 400, 500, and 600 K under 1 mbar of water vapor.

	Core Level	**MoS_2 n-type**	**MoS_2 p-type**	**MoO_3**
Binding Energy (eV)	$Mo3d_{5/2}$	229.26 ± 0.07	228.56 ± 0.07	231.96 ± 0.07
	$S2p_{3/2}$	162.11 ± 0.07	161.41 ± 0.07	-
	O1s	-	-	530.32 ± 0.33

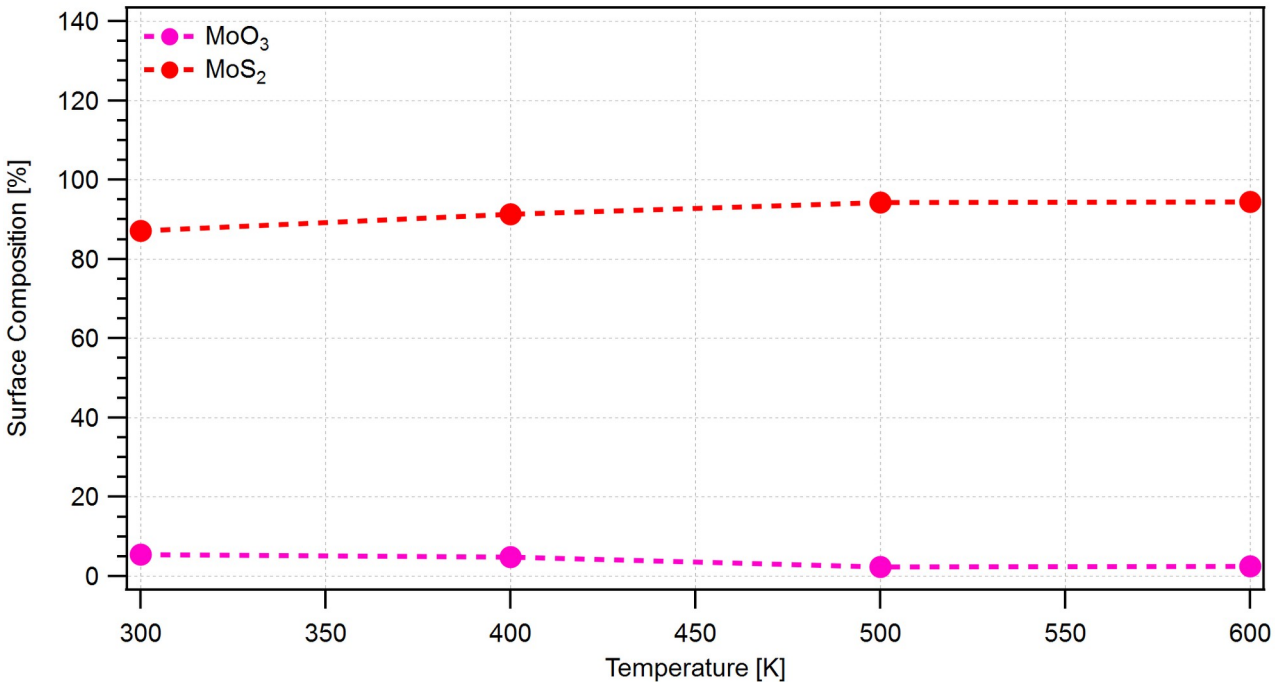

Figure 3.2.2: Calculated surface composition percentages for MoS_2 (red) and MoO_3 (pink) during exposure to 1 mbar of H_2O at 300, 400, 500, and 600 K. The percentage of H_2O (gas phase and adsorbed) is not included. The percentage of MoO_3 does not increase during the experiment, indicating a non-reactive natural MoS_2 surface.

To further confirm the lack of chemical change on the natural MoS_2 surface during the experiment, XPS spectra were collected in ultrahigh vacuum (UHV) conditions before and after the water vapor exposure to compare the differences. Little to no variation was found in the Mo3d and S2p spectra shown in *Figure 3.2.3*. The presence of MoO_3 in this experiment was minimal, making up only 1.8% of the surface composition after the 600 K anneal, and only 0.6% of the surface composition after the 1 mbar of water vapor exposure. The increase after the 600 K anneal, which was intended to degas the sample, was likely caused by the pressure in the chamber increasing too much, allowing oxidation to occur on the surface.

Table 3.2.2: Binding energies of the $Mo3d_{5/2}$, $S2p_{3/2}$, and O1s peaks in *Figure 3.2.3.* The average binding energy was calculated from the fitted spectra after mechanical exfoliation, after annealing to 600 K, and after exposure to 1 mbar of water vapor.

	Core Level	**MoS_2 n-type**	**MoS_2 p-type**	**MoO_3**
Binding Energy (eV)	$Mo3d_{5/2}$	229.38 ± 0.13	228.68 ± 0.13	232
	$S2p_{3/2}$	162.22 ± 0.13	161.52 ± 0.13	-
	O1s	-	-	530.1

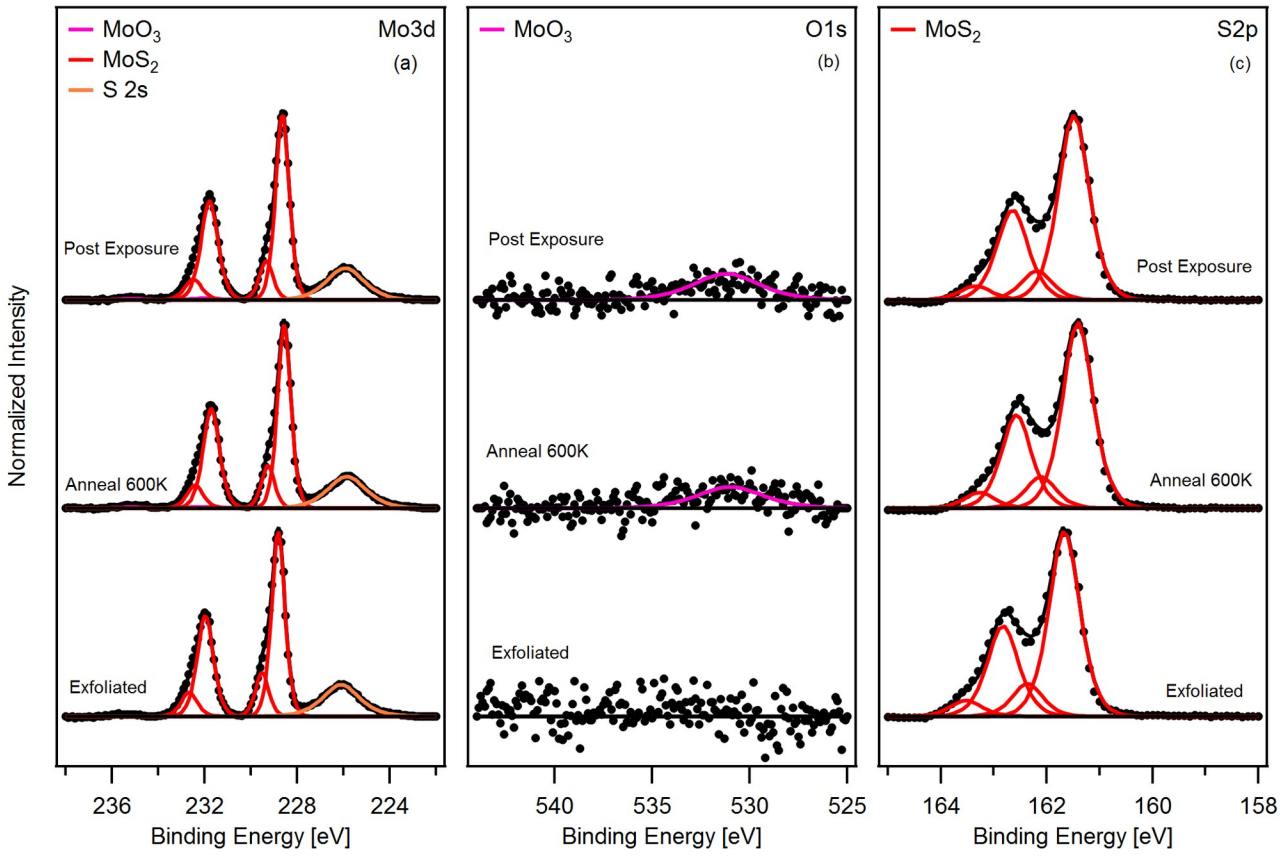

Figure 3.2.3: AP-XPS spectra of an MoS_2 surface after being exfoliated, annealed to 600 K, and after exposure to 1 mbar of water vapor at temperatures ranging from 300-600 K. **(a)** shows the Mo3d core level, **(b)** shows the O1s core level, **(c)** shows the S2p core level. Red peaks represent the MoS_2 species on the surface, the higher binding energy peaks are n-type MoS_2 and lower binding energy peaks are p-type MoS_2. Pink peaks represent MoO_3 on the surface and present themselves at high binding energies in the Mo3d core level spectra.

3.3 $MoS_{1.6}$ Surface

After the MoS_2 surface stoichiometry was reduced to 1.6:1, the sample was exposed to 1 mbar of water vapor at temperatures ranging from 300 K to 600 K in order to determine if the surface had become more chemically active due to the defects. As expected, the surface oxidized through the formation of MoO_3 and MoOS which can be seen in *Figure 3.3.1*. A clear increase in the MoO_3 peak at a binding energy of 531.81 eV can be seen in *Figure 3.3.1b* as well as the MoOS peak at a slightly higher binding energy of 532.3 eV. Simultaneous to the increase in oxidation, the presence of MoS_x also decreased, suggesting that the oxidation occurred at the defects where sulfur and molybdenum were both present and that the MoO_3 forms on the metallic surface and the MoOS forms at the MoS_x edges. The MoOS $Mo3d_{5/2}$ ($S2p_{3/2}$) peak at 229.76 eV (163.08 eV) shows at a slightly higher binding energy than the MoS_2 $Mo3d_{5/2}$ ($S2p_{3/2}$) peak at 229.38 eV (162.22 eV)[19] which is consistent with the Mo^{5+} state as described by Benoist *et al.*[1] The MoS_x $Mo3d_{5/2}$ is found at a lower binding energy[21] of 228.9 eV because the electron cloud of the MoS_x species became more dense around the Mo atom, making it easier for photoelectrons to be generated because of the increased shielding from the positive core. Metallic molybdenum, Mo(0), was also found on the surface with its $Mo3d_{5/2}$ position at 228.27 eV.[12] The low binding energy shoulder that was created through sputtering by the formation of Mo(0) and MoS_x decreased as the surface became oxidized, especially at higher temperatures.

Table 3.3.1: Binding energies of the $Mo3d_{5/2}$, $S2p_{3/2}$, and O1s peaks in *Figure 3.3.1*. The average binding energy was calculated from the fitted spectra at 300, 400, 500, and 600 K under 1 mbar of water vapor.

	Core Level	**MoS_2**	**MoS_x**	**MoO_3**	**MoOS**	**Mo(0)**
Binding Energy (eV)	$Mo3d_{5/2}$	229.38 ± 0.03	228.9 ± 0.07	232.4 ± 0.01	229.76 ± 0.07	228.27 ± 0.04
	$S2p_{3/2}$	162.22 ± 0.07	162.58 ± 0.03	-	163.08 ± 0.3	-
	O1s	-	-	530.81 ± 0.2	532.3 ± 0.28	-

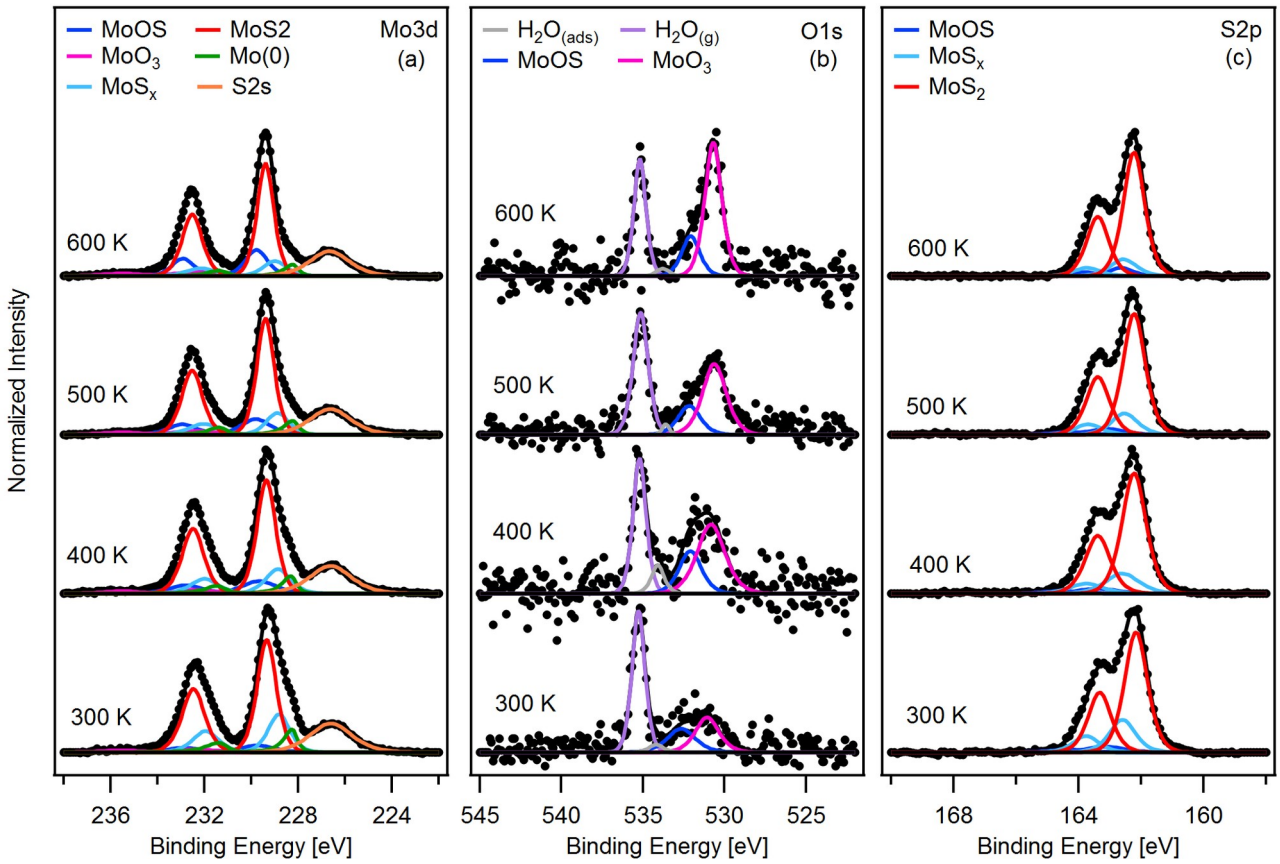

Figure 3.3.1: AP-XPS spectra of a sulfur deficient $MoS_{1.6}$ surface under 1mbar of water vapor at temperatures of 300, 400, 500, and 600 K. **(a)** shows the Mo3d core level, **(b)** shows the O1s core level, **(c)** shows the S2p core level. In the O1s spectra, a clear increase in the MoO_3 (pink) peak and the MoOS (dark blue) peak was seen as temperature increased showing that the surface was oxidizing. The lower binding energy shoulders of the $Mo3d_{5/2}$ and $Mo3d_{3/2}$ peaks decreased with temperature which was caused by the decrease of MoS_x (light blue) and Mo(0) (green) from oxidation.

In *Figure 3.3.2a* the surface composition percentage of each species while exposed to 1 mbar of water vapor was plotted with respect to temperature, where it was seen that MoO_3 and MoOS increased at the similar rates while the percentage of MoS_x and Mo(0) decreased at the same time. In *Figure 3.3.2b*, the overall stoichiometry of the MoS_x species increased which further shows that the oxygen is bonding on the MoS_x edges created by the sputtering process. The O:Mo ratio also quickly returns to the 3:1 state as the surface is exposed to oxygen for more time and higher temperatures, providing more energy to the oxidation reaction.

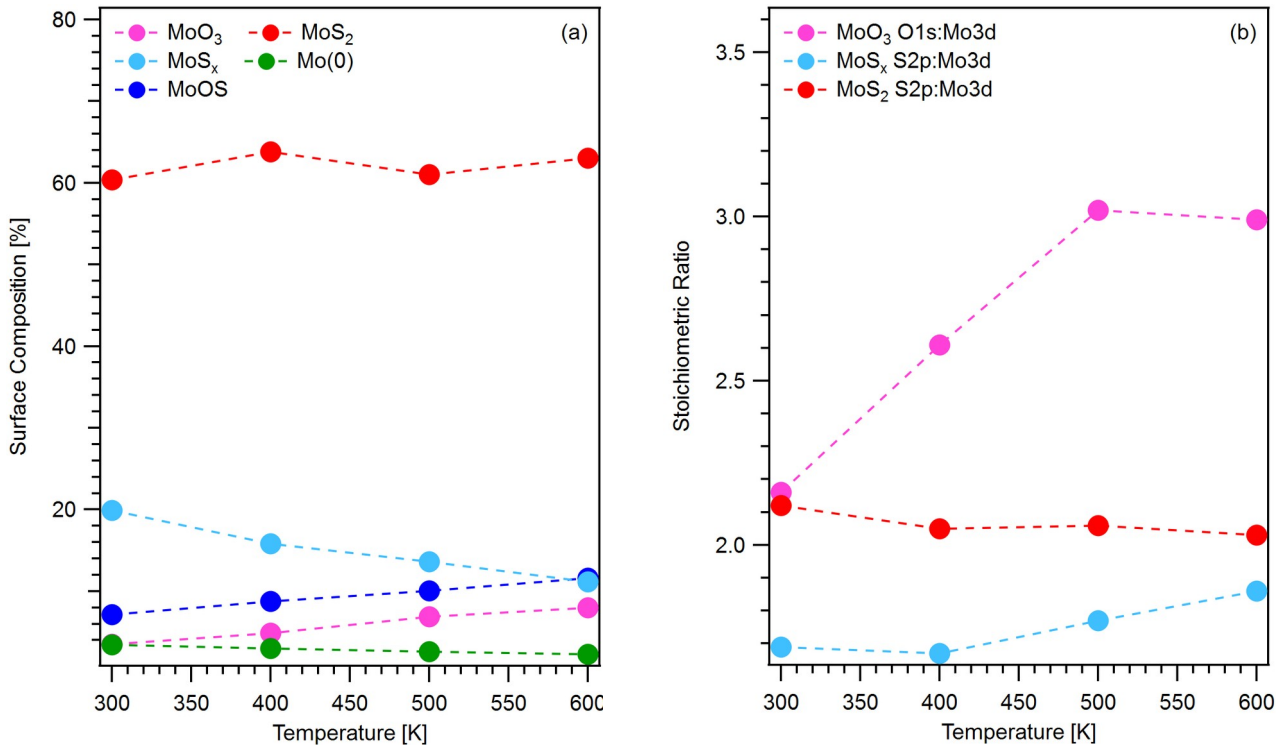

Figure 3.3.2: (a) Calculated surface composition percentages of a defective $MoS_{1.6}$ surface while being exposed to 1 mbar of H_2O vapor at 300, 400, 500, and 600 K. Throughout the experiment the MoO_3 and MoOS percentage increased with temperature, showing that the surface was oxidizing. This corresponded with a decrease in MoS_x showing that the sub-stoichiometric regions were the ones being oxidized, as well as the metallic molybdenum which was also decreasing. **(b)** Calculated stoichiometric ratios of MoO_3 (O:Mo), MoS_2 (S:Mo), and MoS_x (S:Mo). The O:Mo ratio quickly returned to a 3:1 ratio after water exposure showing that the surface was oxidizing, and the S:Mo ratio for the MoS_x increased as the surface became oxidized.

After the water exposure was completed, high resolution XPS spectra were taken under ultra high vacuum (UHV) conditions and were compared to the pre-exposure UHV-XPS spectra. There was a clear change in the O1s core-level in *Figure 3.3.3* between the post-sputtering and post-exposure spectra. After sputtering, there was only a small peak due to $MoO_{1.7}$ present on the surface, where as after exposure, there was a large O1s peak containing MoO_3 at 531.07 eV, MoOS at 532.06 eV, and adsorbed water. The broadness of the Mo3d and S2p core level spectra also decreased because of the reduction of the MoS_x and Mo(0) species on the surface.

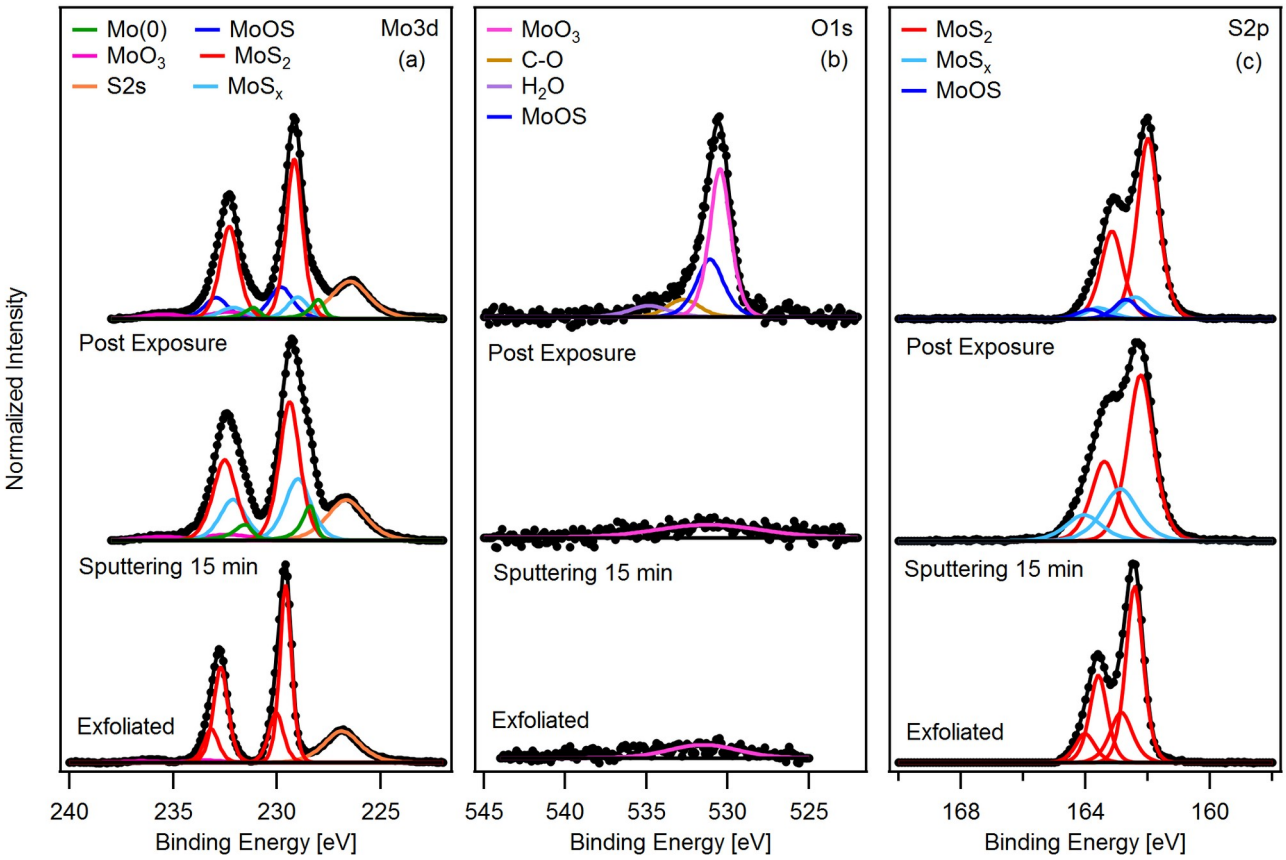

Figure 3.3.3: AP-XPS spectra of a defective $MoS_{1.6}$ surface after being exfoliated, sputtered with Ar^+ ions for 15 minutes, and after exposure to 1 mbar of water vapor at temperatures ranging from 300-600 K. **(a)** shows the Mo3d core-level, **(b)** shows the O1s core level, **(c)** shows the S2p core level. There was a clear difference between the pre and post-exposure spectra for the O1s core level, where a large MoO_3 (pink) peak was seen, as well as a smaller MoOS (dark blue) peak. There was also a increase in the width of the peaks in both the Mo3d and S2p core-level spectra due to the formation of sub-stoichiometric $MoS_{1.6}$ and metallic molybdenum in the case of the Mo3d core-level.

Table 3.3.2: Binding energies of the $Mo3d_{5/2}$, $S2p_{3/2}$, and O1s peaks in *Figure 3.3.3.* The average binding energy was calculated from the fitted spectra after mechanical exfoliation, after 15 minutes of sputtering, and after exposure to 1 mbar of water vapor.

	Core Level	MoS_2	MoS_x	MoO_3	MoOS	Mo(0)
Binding Energy (eV)	$Mo3d_{5/2}$	229.28 ± 0.15	0	232.7 ± 0.6	229.81	228.19 ± 0.29
	$S2p_{3/2}$	162.11 ± 0.17	162.65 ± 0.3	-	162.7	-
	O1s	-	-	531.07 ± 0.46	532.06	-

3.4 $MoS_{1.4}$ Surface

To further confirm that defects to the MoS_2 surface increase its chemical activity, the mechanically exfoliated S:Mo surface stoichiometry of a was reduced to 1.4:1. After which, the sample was exposed to 1 mbar of water vapor at temperatures ranging from 300 K to 600 K to study the oxidation of the surface. Similar to the results found in *Section 3.3*, MoO_3 and MoOS was formed on the surface which can be seen in *Figure 3.4.1.* A clear increase in the MoO_3 peak at a binding energy of 530.38 eV can be seen in *Figure 3.4.1b* as well as the MoOS peak at a slightly higher binding energy of 531.5 eV. Similar to before, the amount of MoS_x character decreased, showing that oxygen is bonding to the MoS*x* edge sites. The metallic character also decreased, representing the formation of Mo-O bonds. The MoOS $Mo3d_{5/2}$ ($S2p_{3/2}$) peak at 229.68[1] eV (162.93 eV) again shows at higher binding energy than the MoS_2 $Mo3d_{5/2}$ ($S2p_{3/2}$) peak at 229.01 eV (161.9 eV).[19] The $Mo3d_{5/2}$ peak corresponding to MoS_x is found at a lower binding energy[21] of 228.65 eV and metallic molybdenum, $Mo3d_{5/2}$ is also found at 228.08 eV[12]. The low binding energy shoulder that was created through sputtering by the formation of Mo(0) and MoS_x decreased as the surface became oxidized. It is also important to note the Sb3d character which has a spin-orbit splitting of 9.4 eV[12] that became apparent in the O1s spectra at higher temperatures. It is more clearly seen in the post exposure spectra discussed later.

Table 3.4.1: Binding energies of the $Mo3d_{5/2}$, $S2p_{3/2}$, and O1s peaks in *Figure 3.4.1.* The average binding energy was calculated from the fitted spectra at 300, 400, 500, and 600 K under 1 mbar of water vapor.

	Core Level	**MoS_2**	**MoS_x**	**MoO_3**	**MoOS**	**Mo(0)**
Binding Energy (eV)	$Mo3d_{5/2}$	229.01 ± 0.08	228.65 ± 0.06	232.34 ± 0.07	229.68 ± 0.11	228.08 ± 0.01
	$S2p_{3/2}$	161.9 ± 0.04	162.44 ± 0.05	-	162.93 ± 0.4	-
	O1s	-	-	530.38 ± 0.07	531.5 ± 0.19	-

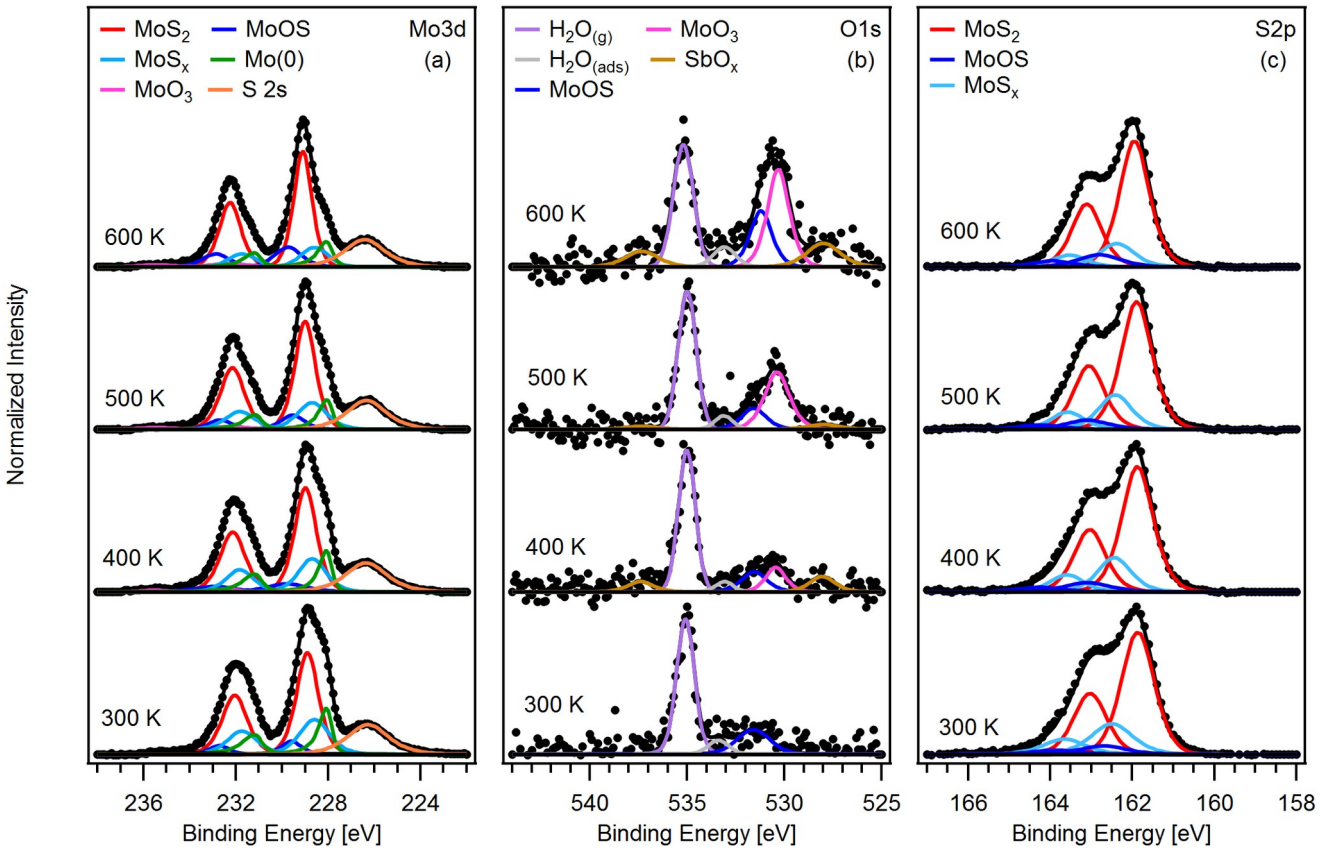

Figure 3.4.1: AP-XPS spectra of a sulfur deficient $MoS_{1.4}$ surface under 1mbar of water vapor at temperatures of 300, 400, 500, and 600 K. **(a)** shows the Mo3d core level, **(b)** shows the O1s core level, **(c)** shows the S2p core level. In the O1s spectra, a clear increase in the MoO_3 (pink) peak and the and MoOS (dark blue) peak was seen as temperature increased showing that the surface was oxidizing. The lower binding energy shoulders of the $Mo3d_{5/2}$ and $Mo3d_{3/2}$ peaks decreased with temperature which was caused by the decrease of MoS_x (light blue) and Mo(0) (green) from oxidation.

In *Figure 3.4.2a* the surface composition percentage of each species while exposed to 1 mbar of water vapor was plotted with respect to temperature, where it was again seen that MoO_3 and MoOS increased at the similar rates while the percentage of MoS_x and Mo(0) decreased at the same time due to the oxidation of the MoS_x defect sites and metallic surface. In *Figure 3.4.2b*, the overall stoichiometry of the MoS_x species increased which further showed that the oxygen is bonding on the MoS_x edges created by the sputtering process. The O:Mo ratio also increased to the 3:1 state as the surface was exposed to oxygen.

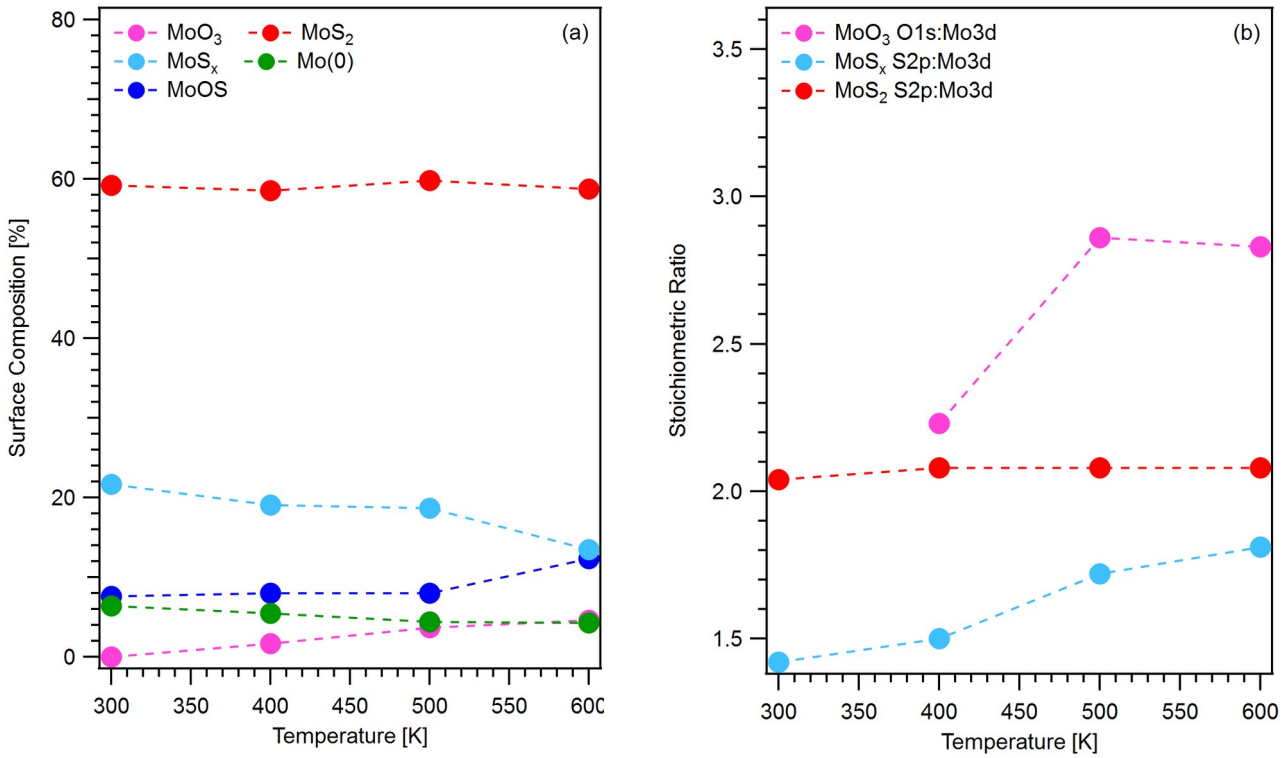

Figure 3.4.2: (a) Calculated surface composition percentages of a defective $MoS_{1.4}$ surface while being exposed to 1 mbar of H_2O vapor at 300, 400, 500, and 600 K. Throughout the experiment the MoO_3 and MoOS percentage increased with temperature, showing that the surface was oxidizing. This corresponded with a decrease in MoS_x showing that the sub-stoichiometric regions were the ones being oxidized, as well as the metallic molybdenum which was also decreasing. **(b)** Calculated stoichiometric ratios of MoO_3 (O:Mo), MoS_2 (S:Mo), and MoS_x (S:Mo). The O:Mo ratio quickly returned to a 3:1 ratio after water exposure showing that the surface was oxidizing, and the S:Mo ratio for the MoS_x increased as the surface became oxidized.

After the water exposure was completed, high resolution XPS spectra were taken under UHV conditions and were compared to the pre-exposure UHV-XPS spectra. There was a clear change in the O1s core-level in *Figure 3.4.3* between the post-sputtering and post-exposure spectra. After sputtering, the C-O and C=O species were successfully removed from the surface, where as after exposure, there was a large O1s peak containing MoO_3 at 530.5 eV, MoOS at 531,4 eV, adsorbed water, and slight character of Sb3d which is distinguished by it 9.4 eV[12] spin-orbit splitting. The broadness of the Mo3d and S2p core level spectra also decreased because of the reduction of the MoS_x and Mo(0) species on the surface.

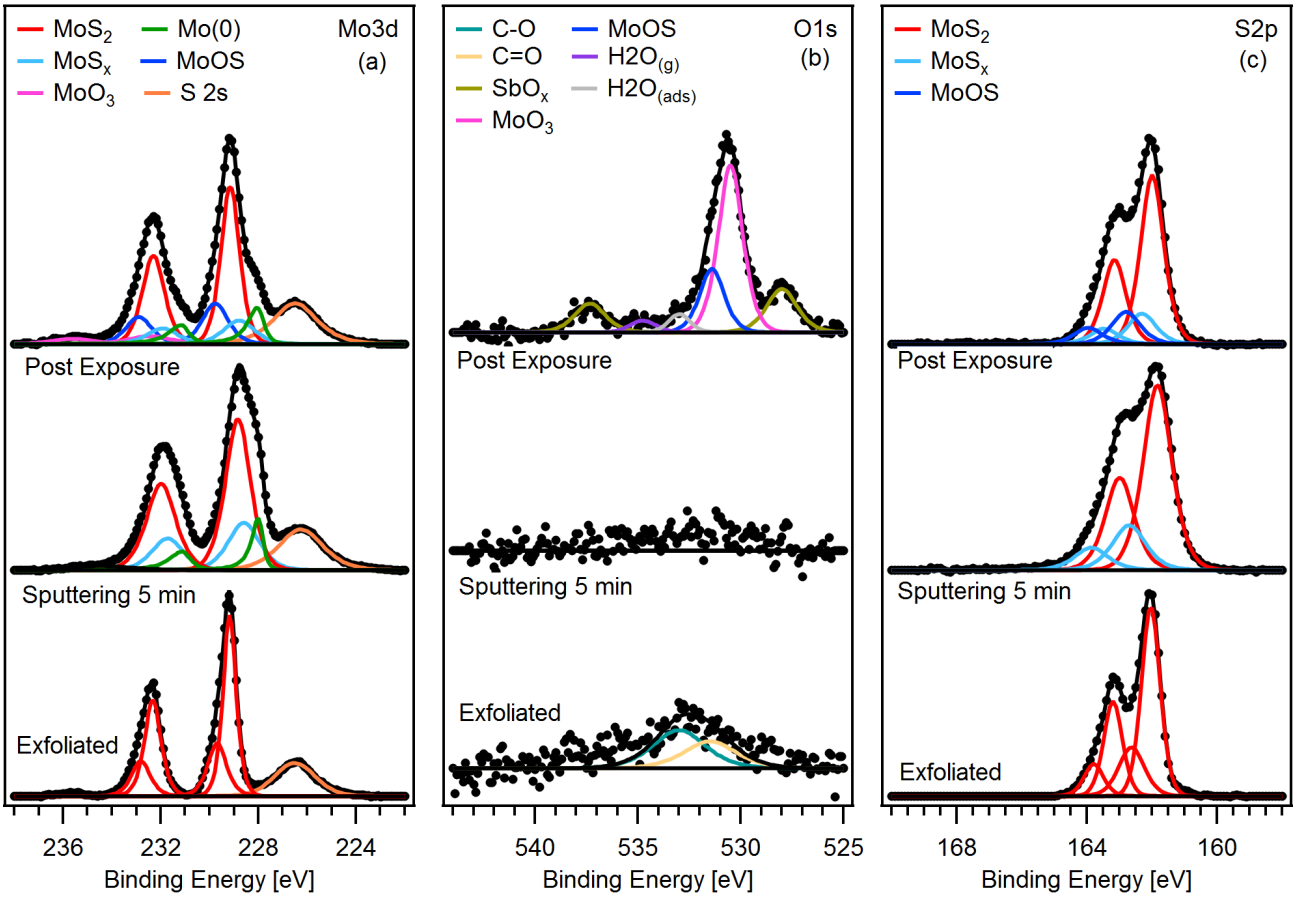

Figure 3.4.3: AP-XPS spectra of a defective $MoS_{1.4}$ surface after being exfoliated, sputtered with Ar^+ ions for 5 minutes, and after exposure to 1 mbar of water vapor at temperatures ranging from 300-600 K. **(a)** shows the Mo3d core-level, **(b)** shows the O1s core level, **(c)** shows the S2p core level. There was a clear difference between the pre and post-exposure spectra for the O1s core level, where a large MoO_3 (pink) peak was seen, as well as a smaller MoOS (dark blue) peak. There was also a increase in the width of the peaks in both the Mo3d and S2p core-level spectra due to the formation of sub-stoichiometric $MoS_{1.6}$ and metallic molybdenum in the case of the Mo3d core-level.

Table 3.4.2: Binding energies of the $Mo3d_{5/2}$, $S2p_{3/2}$, and O1s peaks in *Figure 3.4.3.* The average binding energy was calculated from the fitted spectra after mechanical exfoliation, after 5 minutes of sputtering, and after exposure to 1 mbar of water vapor.

	Core Level	MoS_2	MoS_x	MoO_3	MoOS	Mo(0)
Binding Energy (eV)	$Mo3d_{5/2}$	229.0 ± 0.23	0	232.46	229.78	228.02 ± 0.03
	$S2p_{3/2}$	161.91 ± 0.11	162.51 ± 0.28	-	162.8	-
	O1s	-	-	530.5	531.4	-

3.5 $MoS_{1.2}$ Surface

To observe the oxidation of the most defective surface in this study, the previous $MoS_{1.4}$ sample was further sputtered to a S:Mo ratio to 1.2:1, and was exposed to 1 mbar of water vapor at temperatures ranging from 300 K to 600 K. The expected trends found in *Section 3.3* repeated themselves here through the formation of MoO_3 and MoOS on the surface, as seen in *Figure 3.5.1*. A clear increase in the MoO_3 peak at a binding energy of 530.81 eV was seen in *Figure 3.5.1b* as well as the MoOS peak at a slightly higher binding energy of 532.31 eV. Once again, the amount of MoS_x character decreased, showing that oxygen is bonding to the MoS_x edge sites. The metallic character also decreased due to the formation of Mo-O bonds. The MoOS $Mo3d_{5/2}$ ($S2p_{3/2}$) peak at 229.53[1] eV (162.71 eV) again shows at higher binding energy than the MoS_2 $Mo3d_{5/2}$ ($S2p_{3/2}$) peak at 229.34 eV (162.22 eV).[19] The MoS_x $Mo3d_{5/2}$ is found at a lower binding energy[21] of 228.56 eV and metallic molybdenum, Mo(0), is also found at the surface with its $Mo3d_{5/2}$ position at 228.17 eV.[12] The low binding energy shoulder that was created through sputtering by the formation of Mo(0) and MoS_x decreased as the surface became oxidized.

Table 3.5.1: Binding energies of the $Mo3d_{5/2}$, $S2p_{3/2}$, and O1s peaks in *Figure 3.5.1*. The average binding energy was calculated from the fitted spectra at 300, 400, 500, and 600 K under 1 mbar of water vapor.

	Core Level	**MoS_2**	**MoS_x**	**MoO_3**	**MoOS**	**Mo(0)**
Binding Energy (eV)	$Mo3d_{5/2}$	229.34 ± 0.02	228.56 ± 0.02	231.86 ± 0.11	229.53 ± 0.02	228.17 ± 0.03
	$S2p_{3/2}$	162.22 ± 0.01	162.31 ± 0.07	-	162.71 ± 0.13	-
	O1s	-	-	530.81 ± 0.15	532.31 ± 0.46	-

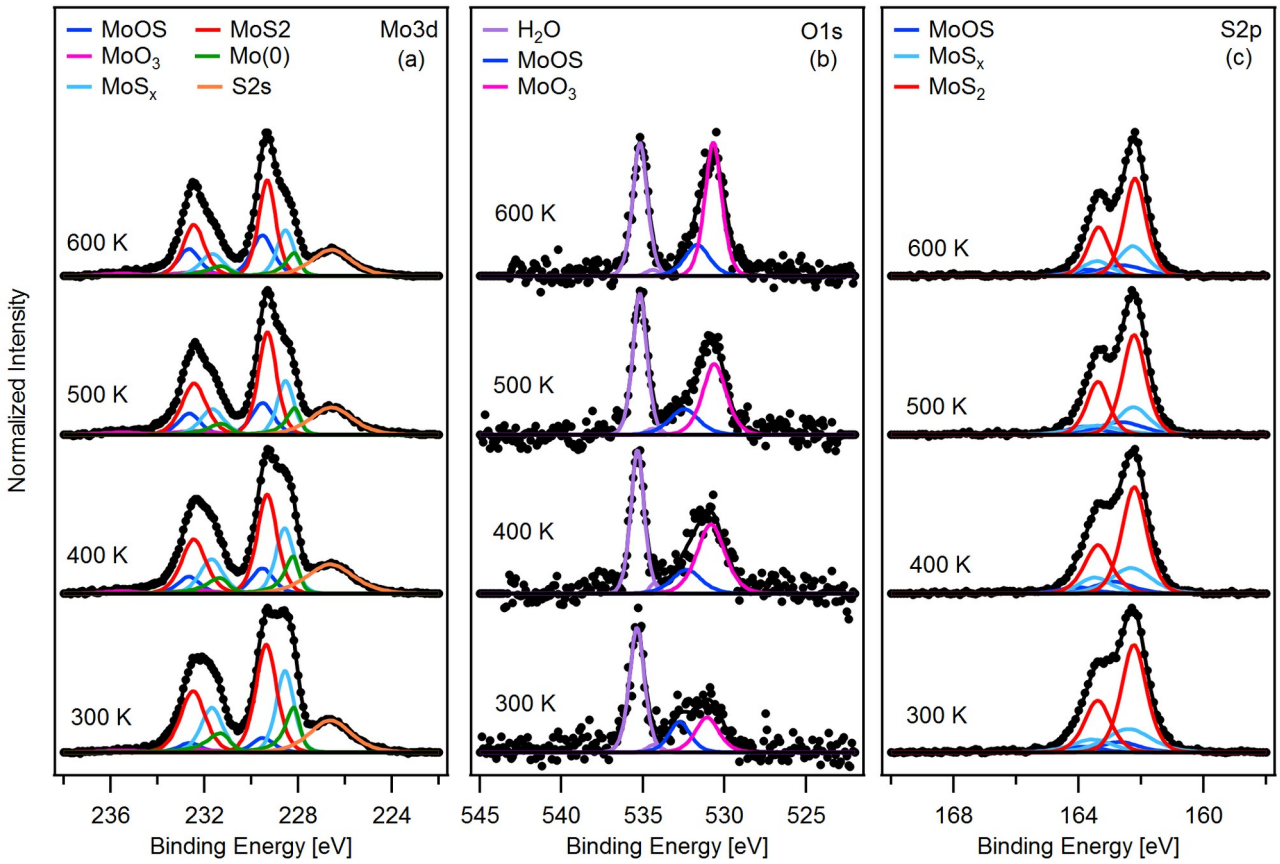

Figure 3.5.1: AP-XPS spectra of a sulfur deficient $MoS_{1.2}$ surface under 1mbar of water vapor at temperatures of 300, 400, 500, and 600 K. **(a)** shows the Mo3d core level, **(b)** shows the O1s core level, **(c)** shows the S2p core level. In the O1s spectra, a clear increase in the MoO_3 (pink) peak and the and MoOS (dark blue) peak was seen as temperature increased showing that the surface was oxidizing. The lower binding energy shoulders of the $Mo3d_{5/2}$ and $Mo3d_{3/2}$ peaks decreased with temperature which was caused by the decrease of MoS_x (light blue) and Mo(0) (green) from oxidation.

In *Figure 3.5.2a* the surface composition percentage of each species while exposed to 1 mbar of water vapor was plotted with respect to temperature, where it was again seen that MoO_3 and MoOS increased at the similar rates while the percentage of MoS_x and Mo(0) decreased at the same time due to the oxidation of the MoS_x defect sites and metallic surface. In *Figure 3.5.2b*, the overall stoichiometry of the MoS_x species once again increased and the O:Mo ratio also increased to the 3:1 state.

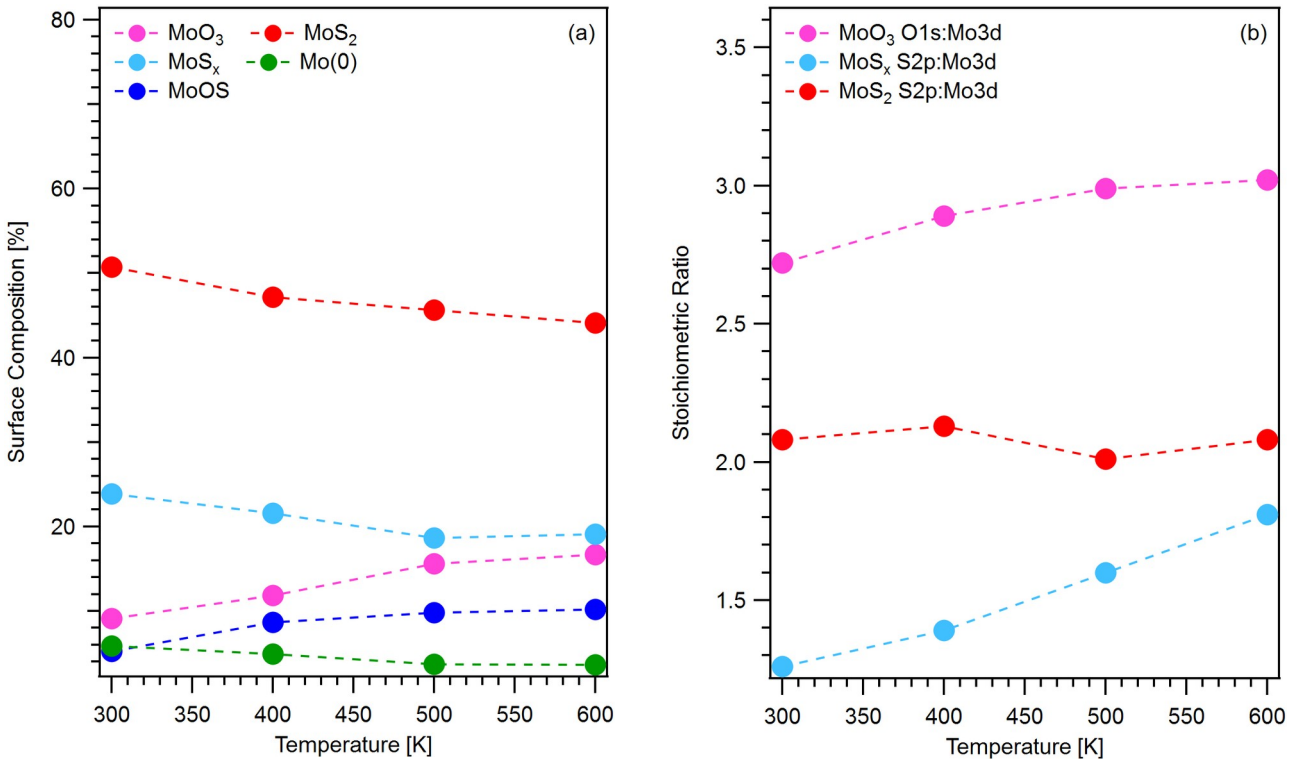

Figure 3.5.2: (a) Calculated surface composition percentages of a defective $MoS_{1.2}$ surface while being exposed to 1 mbar of H_2O vapor at 300, 400, 500, and 600 K. Throughout the experiment the MoO_3 and MoOS percentage increased with temperature, showing that the surface was oxidizing. This corresponded with a decrease in MoS_x showing that the sub-stoichiometric regions were the ones being oxidized, as well as the metallic molybdenum which was also decreasing. **(b)** Calculated stoichiometric ratios of MoO_3 (O:Mo), MoS_2 (S:Mo), and MoS_x (S:Mo). The O:Mo ratio quickly returned to a 3:1 ratio after water exposure showing that the surface was oxidizing, and the S:Mo ratio for the MoS_x increased as the surface became oxidized.

After the water exposure was completed, high resolution XPS spectra where taken under ultra high vacuum (UHV) conditions and were compared to the pre-exposure UHV-XPS spectra. There was a slight change in the O1s core-level in *Figure 3.5.3* between the initial sputtering spectra and the final sputtering spectra. Since this surface was taken directly after the oxidation of the $MoS_{1.4}$ there was already a presence of MoO_3 (530.44 eV) and MoOS (532.83 eV) in the O1s spectra, however, after the exposure, the signal to noise ratio was decreased greatly, which means there are stronger oxide peaks. The broadness of the Mo3d and S2p core level spectra also decreased because of the reduction of the MoS_x and Mo(0) species on the surface.

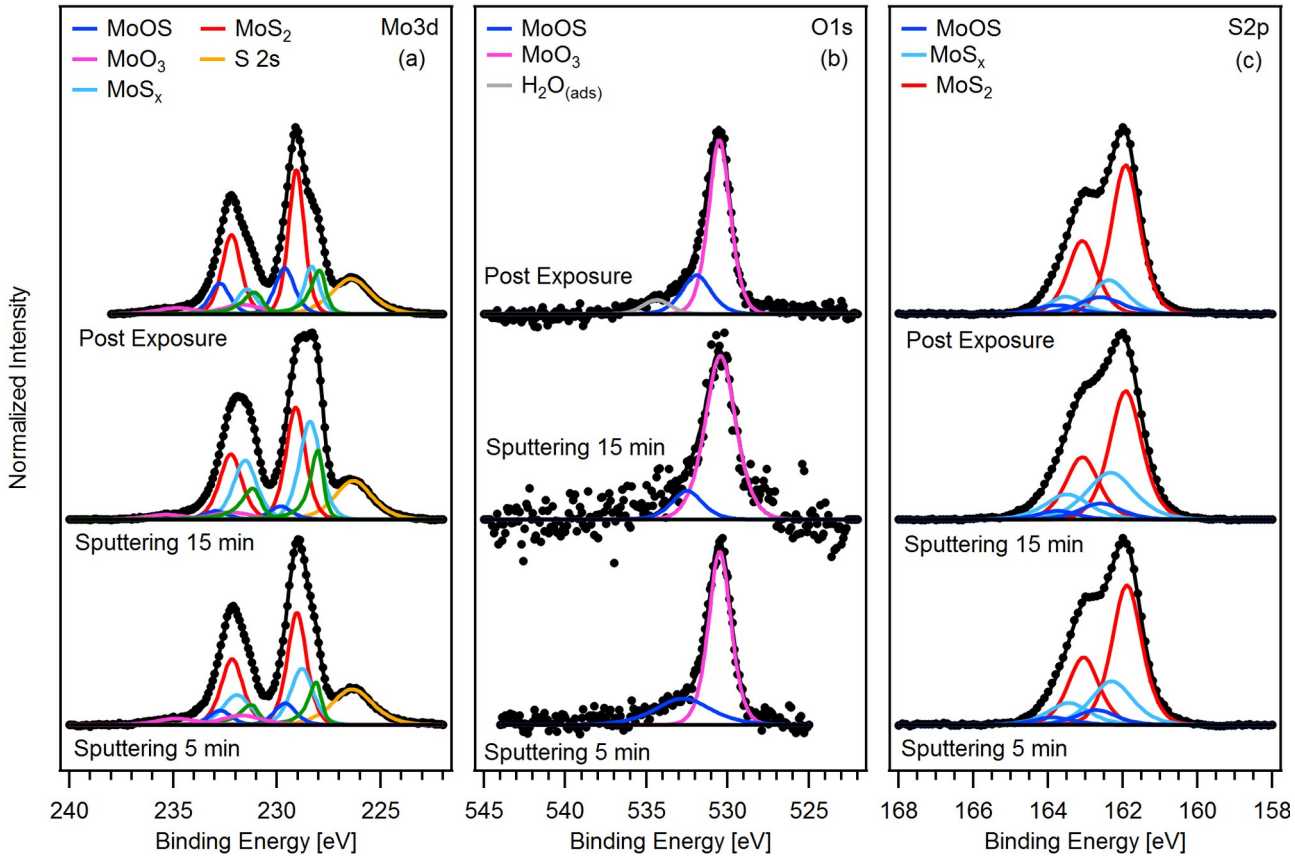

Figure 3.5.3: AP-XPS spectra of a defective $MoS_{1.2}$ surface after being sputtered with Ar^+ ions for 5 minutes, 15 minutes, and after exposure to 1 mbar of water vapor at temperatures ranging from 300-600 K. **(a)** shows the Mo3d core-level, **(b)** shows the O1s core level, **(c)** shows the S2p core level. There was a clear difference between the pre and post-exposure spectra for the O1s core level, where a large MoO_3 (pink) peak was seen, as well as a smaller MoOS (dark blue) peak. There was also a increase in the width of the peaks in both the Mo3d and S2p core-level spectra due to the formation of sub-stoichiometric $MoS_{1.6}$ and metallic molybdenum in the case of the Mo3d core-level.

Table 3.5.2: Binding energies of the $Mo3d_{5/2}$, $S2p_{3/2}$, and O1s peaks in *Figure 3.5.3.* The average binding energy was calculated from the fitted spectra after 5 minutes of sputtering, 15 minutes of sputtering, and after exposure to 1 mbar of water vapor.

	Core Level	MoS_2	MoS_x	MoO_3	MoOS	Mo(0)
Binding Energy (eV)	$Mo3d_{5/2}$	229.07 ± 0.03	228.52 ± 0.25	231.86 ± 0.21	229.68 ± 0.09	228.05 ± 0.04
	$S2p_{3/2}$	161.91 ± 0.01	162.35 ± 0.04	-	162.68 ± 0.08	-
	O1s	-	-	530.44 ± 0.03	532.83 ± 0.27	-

3.6 Discussion

To compare all the surfaces discussed above, the Mo3d core level XPS spectra after the completion of sputtering and or annealing were normalized and plotted next to each other in *Figure 3.6.1*. The lower binding energy shoulder became more clear and prominent as the S:Mo ratio decreased due to the formation of the MoS_x and Mo(0) species. For future experiments, the size and shape of the lower binding energy shoulder could be a qualitative way of preparing surface defects on other MoS_2 samples for HER experiments.

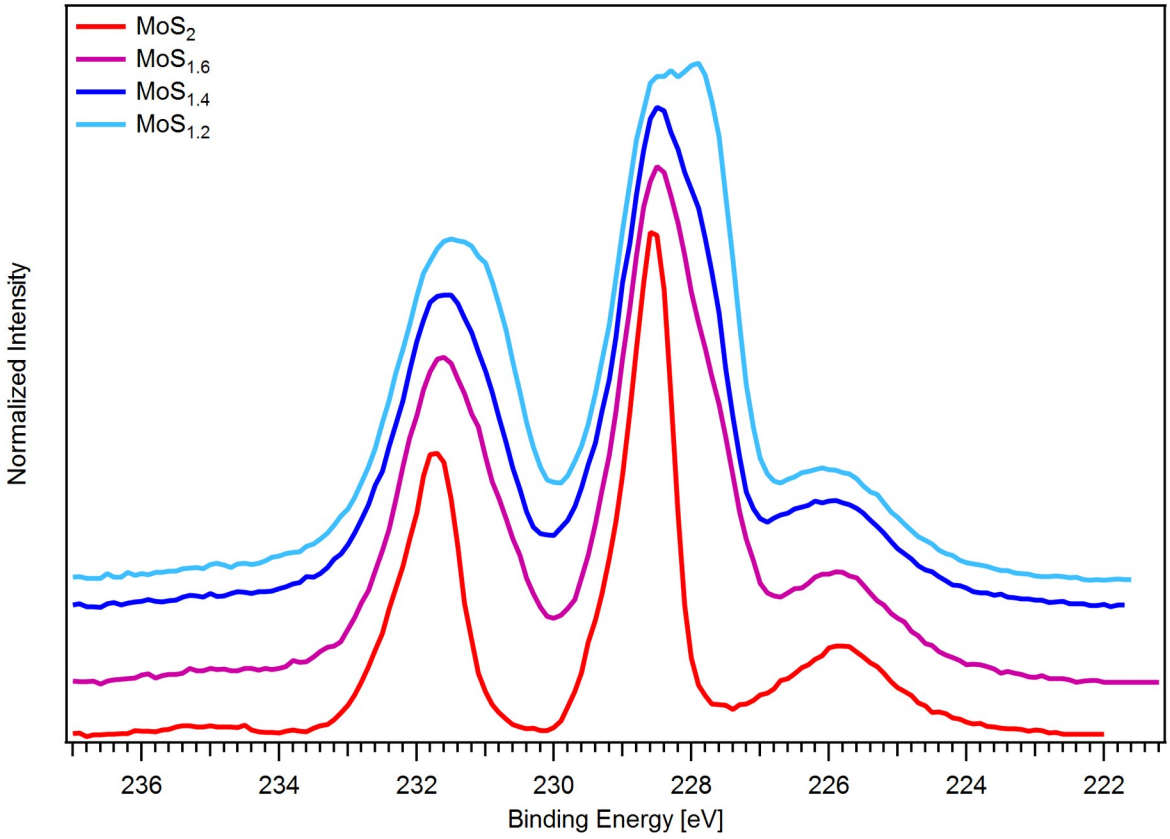

Figure 3.6.1: Mo3d core level XPS spectra of the MoS_2, $MoS_{1.6}$, $MoS_{1.4}$, and $MoS_{1.2}$ surfaces after defects are induced with argon ion sputtering and before exposure to 1 mbar water vapor. At the S:Mo ratio decreased, the lower binding energy shoulder increased due to the presence of MoS_x and Mo(0) on the surface.

Figure 3.6.2a shows the surface composition percentage of MoS_x for each defective surface discussed in sections *3.3-3.5*. The $MoS_{1.2}$ sample naturally had more MoS_x on the surface, which seconds the quantitative understanding of *Figure 3.6.1*. As the temperature increased, the amount of MoS_x decreased and the stoichiometry (*Figure 3.6.2b*) increased because oxygen was bonding to the exposed Mo-S edges, creating new oxidation states.

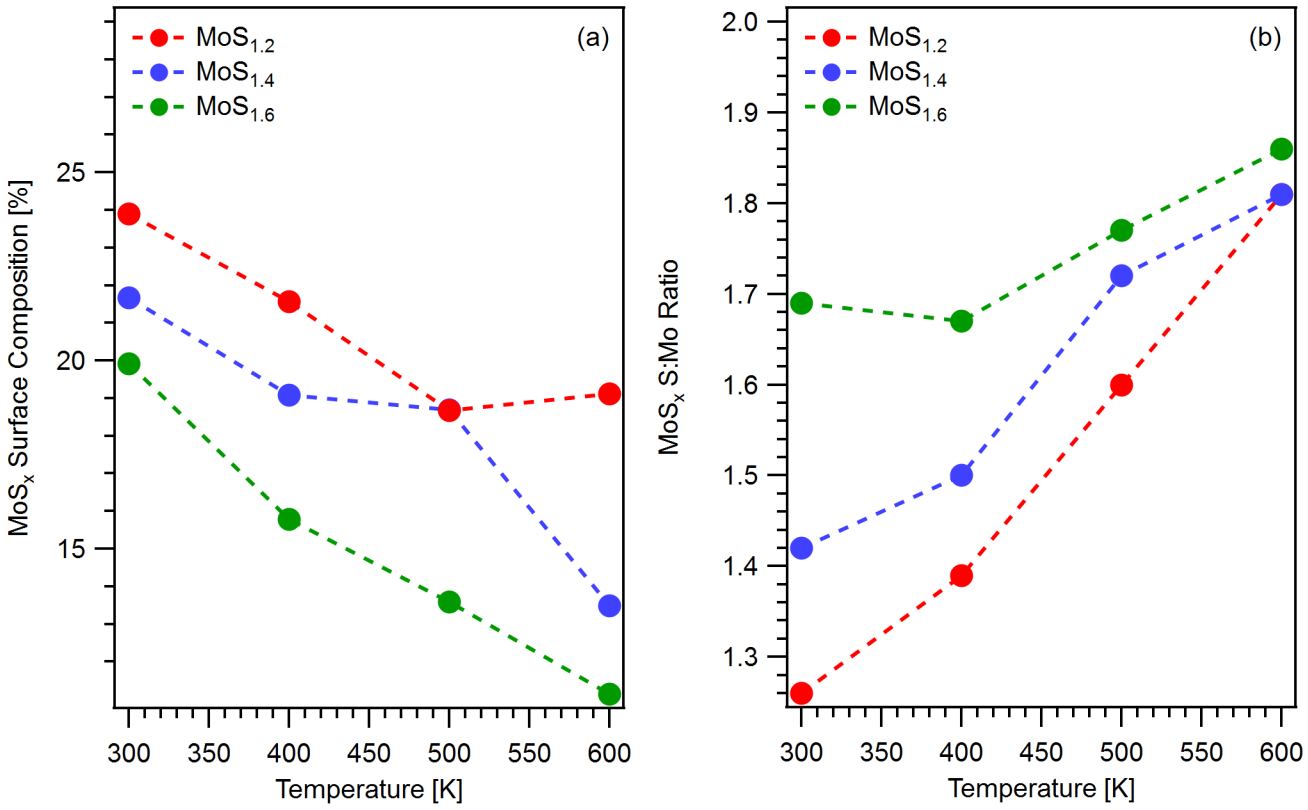

Figure 3.6.2: (a) Calculated surface composition percentages of MoS_x on the three defective surfaces discussion above while being exposed to 1 mbar of H_2O vapor at 300, 400, 500, and 600 K. Throughout the experiment the MoS_x decreased because it was being oxidized to the MoOS state. The MoS_x on each surface decreased at similar rates. **(b)** Calculated stoichiometric ratios of MoS_x (S:Mo) for the three defective surfaces discussed above. The S:Mo ratio increased as the surface became oxidized, and all three surfaces eventually reached a S:Mo ratio of ~1.8.

The oxidation of the surface is understood by calculating the surface composition percentages of each oxide species with respect to temperature during the 1 mbar of water exposure. Both the MoO_3 (*Figure 3.6.3a*) and MoOS (*Figure 3.6.3b*) showed increasing oxidation with respect to temperature.

For the MoO_3, the more defective surfaces resulted in more oxidation found on the surface. To compare the MoO_3 percentages directly, the values for each different surface were offset to force the value at 300 K to be zero. This was necessary for direct comparison because the $MoS_{1.2}$ and $MoS_{1.6}$ surfaces had a native oxide present on the surface where as the $MoS_{1.4}$ surface did not.

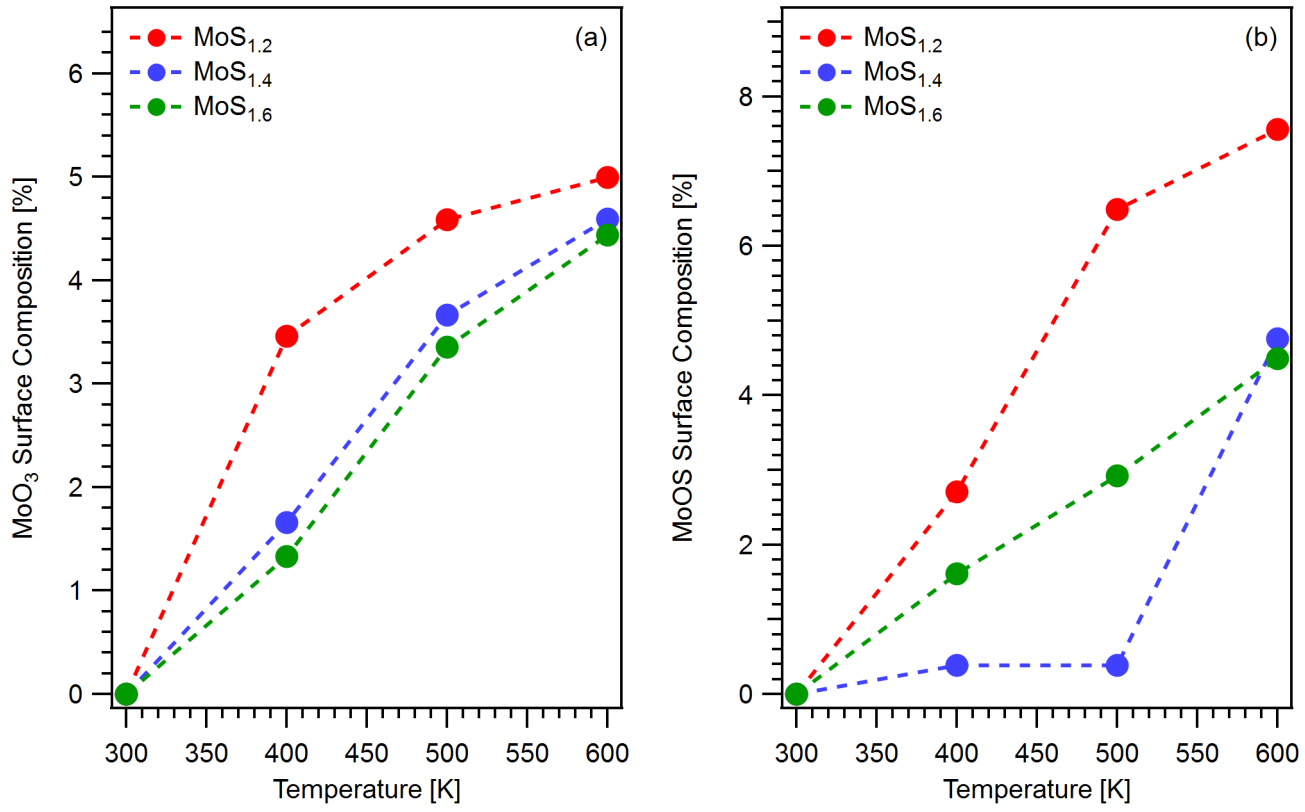

Figure 3.5.2: (a) Calculated surface composition percentages of MoO_3 on the three defective surfaces discussion above while being exposed to 1 mbar of H_2O vapor at 300, 400, 500, and 600 K. Since each sample had a different amount of native oxide on the surface, the values were offset to force the first point to start at zero to allow for a direct comparison between all samples. As expected, more defective surface led to more oxidation. **(b)** Calculated surface composition percentages of MoOS on the three defective surfaces discussion above while being exposed to 1 mbar of H_2O vapor at 300, 400, 500, and 600 K. Similar to the MoO_3, the more defective surfaces led to the formation of more MoOS.

4. Conclusions and Perspectives

In summary, it was shown that the basal plane of MoS_2 can be effectively activated through the removal of surface sulfur atoms via argon ion sputtering. As more sulfur is removed from the top layer of the material, distinctive lower binding energy shoulders will appear in the Mo3d core level XPS spectra which arises from the sulfur deficient MoS_x and metallic molybdenum which is formed on the surface. When exposed to 1 mbar of water vapor at different temperatures oxygen will bond to either the sulfur deficient MoS_x and form MoOS or it will bond to the metallic molybdenum and form MoO_3. To fully understand the benefit of defects on HER performance, further electocatalytic experiments can be performed such as cyclic voltometry to characterize the tafel slope and active surface area of the MoS_2 samples with varying amounts of defects. Positive results from these experiments can prove MoS_2 to be useful as a possible cheap alternative to platinum for an HER catalyst.

5. Acknowledgments

Acquisition of the Ambient-Pressure X-ray Photoelectron Spectroscopy/Ambient-Pressure Scanning Tunneling Microscopy system was supported by the National Science Foundation-Major Research Instrumentation program (grant DMR-1429765), the M. J. Murdock Charitable Trust, Oregon BEST, Oregon Nanoscience and Microtechnologies Institute, and Oregon State University.

6. Bibliography

(1) Benoist, L.; Gonbeau, D.; Pfister-Guillouzo, G.; Schmidt, E.; Meunier, G.; Levasseur, A. X-Ray Photoelectron Spectroscopy Characterization of Amorphous Molybdenum Oxysulfide Thin Films. *Thin Solid Films* **1995**, *258* (1–2), 110–114. https://doi.org/10.1016/0040-6090(94)06383-4.

(2) Hu, Z.; Wu, Z.; Han, C.; He, J.; Ni, Z.; Chen, W. Two-Dimensional Transition Metal Dichalcogenides: Interface and Defect Engineering. *Chem. Soc. Rev.* **2018**, *47* (9), 3100–3128.

(3) Hus, S. M.; Li, A.-P. Spatially-Resolved Studies on the Role of Defects and Boundaries in Electronic Behavior of {2D} Materials. *Prog. Surf. Sci.* **2017**, *92* (3), 176–201.

(4) Li, J.; Kang, J.; Cai, Q.; Hong, W.; Jian, C.; Liu, W.; Banerjee, K. Boosting Hydrogen Evolution Performance of MoS2 by Band Structure Engineering. *Adv. Mater. Interfaces* **2017**, *4* (16), 1700303. https://doi.org/10.1002/admi.201700303.

(5) Mas-Balleste, R.; Gomez-Navarro, C.; Nanoscale, J. G.-H.-; 2011, undefined. 2D Materials: To Graphene and Beyond. *pubs.rsc.org*.

(6) Novoselov, K.; Mishchenko, A.; Science, A. C.-; 2016, undefined. 2D Materials and van Der Waals Heterostructures. *science.sciencemag.org*.

(7) Léger, J.-M.; Hahn, F. Chapter 3 - Contribution of In-Situ Infrared Reflectance Spectroscopy in the Study of Nanostructured Fuel Cell Electrodes. In *In-situ {Spectroscopic} {Studies} of {Adsorption} at the {Electrode} and {Electrocatalysis}*; Sun, S.-G., Christensen, P. A., Wieckowski, A., Eds.; Elsevier Science B.V.: Amsterdam, 2007; pp 63–98. https://doi.org/10.1016/B978-044451870-5/50004-X.

(8) Li, H.; Tsai, C.; Koh, A.; Cai, L.; materials, A. C.-N.; 2016, undefined. Activating and Optimizing MoS2 Basal Planes for Hydrogen Evolution through the Formation of Strained Sulphur Vacancies. *nature.com*.

(9) Sun, T.; Zhang, G.; Xu, D.; Lian, X.; Li, H.; Chen, W.; Su, C. Defect Chemistry in 2D Materials for Electrocatalysis. *Materials Today Energy*. Elsevier Ltd June 1, 2019, pp 215–238. https://doi.org/10.1016/j.mtener.2019.01.004.

(10) Tang, Q.; Jiang, D. E. Mechanism of Hydrogen Evolution Reaction on 1T-MoS2 from First Principles. *ACS Catal.* **2016**, *6* (8), 4953–4961. https://doi.org/10.1021/acscatal.6b01211.

(11) Liu, P.; Zhu, J.; Zhang, J.; Xi, P.; Tao, K.; Gao, D.; Xue, D. P Dopants Triggered New Basal Plane Active Sites and Enlarged Interlayer Spacing in MoS2 Nanosheets toward Electrocatalytic Hydrogen Evolution. *ACS Energy Lett.* **2017**, *2* (4), 745–752. https://doi.org/10.1021/acsenergylett.7b00111.

(12) Chastain, J. Handbook of X-Ray Photoelectron Spectroscopy. *Perkin-Elmer Corp.* **1992**, *40*, 221.

(13) Cumpson, P. J.; Seah, M. P. Elastic Scattering Corrections in AES and XPS. II. Estimating Attenuation Lengths and Conditions Required for Their Valid Use in Overlayer/Substrate Experiments. *Surf. Interface Anal.* **1997**, *25* (6), 430–446. https://doi.org/10.1002/(SICI)1096-9918(199706)25:6<430::AID-SIA254>3.0.CO;2-7.

(14) theory, C. F.-E. spectroscopy:; techniques, undefined; 1978, undefined. Basic Concepts of X-Ray Photoelectron Spectroscopy. *Acad. Press New York*.

(15) Yeh, J. J.; Lindau, I. Atomic Subshell Photoionization Cross Sections and Asymmetry Parameters: 1 ≤ {Z} ≤ 103. *At. data Nucl. data tables* **1985**, *32* (1), 1–155.

(16) Langhorne, J. Y.-; (USA), P.; 1993, undefined. Atomic Calculation of Photoionization Cross-Section and Asymmetry Parameters Gordon and Breach Science Publishers.

(17) Baltrusaitis, J.; Mendoza-Sanchez, B.; Fernandez, V.; Veenstra, R.; Dukstiene, N.; Roberts, A.; Fairley, N. Generalized Molybdenum Oxide Surface Chemical State XPS Determination via Informed Amorphous Sample Model. *Appl. Surf. Sci.* **2015**, *326*, 151–161. https://doi.org/https://doi.org/10.1016/j.apsusc.2014.11.077.

(18) Addou, R.; Colombo, L.; Wallace, R. M. Surface Defects on Natural MoS2. *ACS Appl. Mater. Interfaces* **2015**, *7* (22), 11921–11929. https://doi.org/10.1021/acsami.5b01778.

(19) Ganta, D.; Sinha, S.; Haasch, R. 2-D Material Molybdenum Disulfide Analyzed by XPS. *Surf. Sci. Spectra* **2014**, *21*. https://doi.org/10.1116/11.20140401.

(20) Addou, R.; McDonnell, S.; Barrera, D.; Guo, Z.; Azcatl, A.; Wang, J.; Zhu, H.; Hinkle, C. L.; Quevedo-Lopez, M.; Alshareef, H. N.; Colombo, L.; Hsu, J. W. P.; Wallace, R. M. Impurities and Electronic Property Variations of Natural MoS2 Crystal Surfaces. *ACS Nano* **2015**, *9* (9), 9124–9133. https://doi.org/10.1021/acsnano.5b03309.

(21) Baker, M. A.; Gilmore, R.; Lenardi, C.; Gissler, W. XPS Investigation of Preferential Sputtering of S from MoS2 and Determination of MoSx Stoichiometry from Mo and S Peak Positions. *Appl. Surf. Sci.* **1999**, *150* (1), 255–262. https://doi.org/https://doi.org/10.1016/S0169-4332(99)00253-6.